



Dot/Icm-Dependent Restriction of *Legionella pneumophila* within Neutrophils

Christopher T. D. Price,^a Hannah E. Hanford,^a Aruna Vashishta,^b Mateja Ozanic,^c Marina Santic,^{c,e} Silvia Uriarte,^a Yousef Abu Kwaik^{a,d}

^aDepartment of Microbiology and Immunology, University of Louisville, Louisville, Kentucky, USA

^bDepartment of Medicine, University of Louisville, Louisville, Kentucky, USA

^cUniversity of Rijeka, Rijeka, Croatia

^dCenter for Predictive Medicine, College of Medicine, University of Louisville, Louisville, Kentucky, USA

^eUniversity of Rijeka, Faculty of Medicine, Department of Microbiology and Parasitology, Rijeka, Croatia

Christopher T.D. Price and Hannah E. Hanford contributed equally to this work. Christopher T.D. Price initiated the research and is listed first.

ABSTRACT The Dot/Icm type IV secretion system (T4SS) of *Legionella pneumophila* is essential for lysosomal evasion and permissiveness of macrophages for intracellular proliferation of the pathogen. In contrast, we show that polymorphonuclear cells (PMNs) respond to a functional Dot/Icm system through rapid restriction of *L. pneumophila*. Specifically, we show that the *L. pneumophila* T4SS-injected amylase (LamA) effector catalyzes rapid glycogen degradation in the PMNs cytosol, leading to cytosolic hyperglucose. Neutrophils respond through immunometabolic reprogramming that includes upregulated aerobic glycolysis. The PMNs become activated with spatial generation of intracellular reactive oxygen species within the *Legionella*-containing phagosome (LCP) and fusion of specific and azurophilic granules to the LCP, leading to rapid restriction of *L. pneumophila*. We conclude that in contrast to macrophages, PMNs respond to a functional Dot/Icm system, and specifically to the effect of the injected amylase effector, through rapid engagement of major microbicidal processes and rapid restriction of the pathogen.

IMPORTANCE *Legionella pneumophila* is commonly found in aquatic environments and resides within a wide variety of amoebal hosts. Upon aerosol transmission to humans, *L. pneumophila* invades and replicates with alveolar macrophages, causing pneumonia designated Legionnaires' disease. In addition to alveolar macrophages, neutrophils infiltrate into the lungs of infected patients. Unlike alveolar macrophages, neutrophils restrict and kill *L. pneumophila*, but the mechanisms were previously unclear. Here, we show that the pathogen secretes an amylase (LamA) enzyme that rapidly breakdowns glycogen stores within neutrophils, and this triggers increased glycolysis. Subsequently, the two major killing mechanisms of neutrophils, granule fusion and production of reactive oxygen species, are activated, resulting in rapid killing of *L. pneumophila*.

KEYWORDS reactive oxygen species, granules, phagosome, polymorphonuclear leukocytes

Legionella pneumophila is an aquatic organism that has evolved to proliferate within a wide range of amoebae species as its primary hosts (1–4). While amoebae and other protists are the natural hosts for *L. pneumophila*, humans can become an accidental host through inhalation of contaminated environmental aerosols (5, 6). Upon inhalation, the organism invades alveolar macrophages via coiling phagocytosis (7, 8) and begins to proliferate, resulting in pneumonia designated Legionnaires' disease

Citation Price CTD, Hanford HE, Vashishta A, Ozanic M, Santic M, Uriarte S, Kwaik YA. 2021. Dot/Icm-dependent restriction of *Legionella pneumophila* within neutrophils. *mBio* 12: e01008-21. <https://doi.org/10.1128/mBio.01008-21>.

Editor Nancy E. Freitag, University of Illinois at Chicago

Copyright © 2021 Price et al. This is an open-access article distributed under the terms of the [Creative Commons Attribution 4.0 International license](https://creativecommons.org/licenses/by/4.0/).

Address correspondence to Yousef Abu Kwaik, abukwaik@louisville.edu.

This article is a direct contribution from Yousef Abu Kwaik, a Fellow of the American Academy of Microbiology, who arranged for and secured reviews by Ralph Isberg, Tufts Medical School; Thomas Rudel, University of Wuerzburg; and Jason Carolyn, University of West VA.

Received 8 April 2021

Accepted 12 April 2021

Published 26 May 2021

(9–11). The Dot/Icm type IV translocation system of *L. pneumophila*, which functions as a molecular syringe, injects ~350 different protein effectors into the host cell cytosol to evade lysosomal fusion and overrides restriction of pathogen proliferation in both amoebae and alveolar macrophages (12–19).

Various intracellular pathogens have evolved to evade the innate immune response of macrophages (20–22) where they manipulate processes such as vesicle traffic, the lysosomal degradation pathway (23, 24), and the innate immune pathogen sensing mechanisms (25–28). However, neutrophils or polymorphonuclear leukocytes (PMNs) are largely restrictive to most pathogens with very few exceptions. In addition to alveolar macrophages, PMNs are present in the alveoli of pulmonary biopsy specimens from patients and experimental animals infected with *L. pneumophila*. Since 1981, PMNs have been reported to restrict *L. pneumophila*, and several studies *in vivo* in mice have shown that PMNs are required for the rapid innate defense in controlling the *L. pneumophila* infection (12, 14, 16–18, 29–35). Almost 4 decades later, the mechanisms of pathogen uptake and restriction within PMNs remain unknown. PMNs account for 50 to 60% of peripheral blood leukocytes in humans and are an essential part of the innate immune defense against microbial infections.

Upon infection of macrophages and amoeba hosts by *L. pneumophila*, the Dot/Icm-injected repertoire of effectors is involved in manipulation of various host cell processes to remodel the macrophage into a proliferation niche (6, 36–41). Although *L. pneumophila* injects Dot/Icm effectors into the cytosol of PMNs (17), proliferation of the pathogen is restricted in PMNs (12–19, 42). Thus, the ability of PMNs to restrict *L. pneumophila* proliferation is very different from the permissiveness of macrophages. In mice, infiltrating PMNs in the mouse lungs respond to the effect of Dot/Icm translocation of effectors through the secretion of many proinflammatory cytokines, including interleukin 1 alpha (IL-1 α), tumor necrosis factor alpha (TNF- α), IL-12, and IL-17 (12, 14, 16–18). In addition, the release of PMNs proinflammatory cytokines has a paracrine effect on PMNs and macrophages that amplify the inflammatory response and enhance pathogen restriction and clearance (43, 44).

Neutrophil extracellular traps (NETs) have been thought to contribute to pathogen-killing mechanisms by PMNs (45–47). However, the two major antimicrobial arms of PMNs are the generation of reactive oxygen species (ROS) by the phagocyte NADPH oxidase and the antimicrobial matrix contents of the specific and azurophilic granules (44). In quiescent PMNs, NADPH oxidase is kept inactive through compartmentalization of three membrane subunits (gp91phox/NOX2, p22phox, and Rap1A) and four cytosolic proteins (p47phox, p67phox, p40phox, and Rac2). Upon stimulation, the cytosolic subunits translocate to the membrane to form the catalytically active enzyme complex, which generates the ROS (48–54). The specific granules contain several antimicrobial proteins like cathelicidin, lactoferrin, and lysozyme, while the azurophilic granules contain the potent cationic antimicrobial peptides α -defensins, myeloperoxidase, proteinase 3, and elastase, among others (43, 44). Although restriction of *L. pneumophila* was reported since 1981, the mechanism remained unknown (55). It is not known whether any of the two major PMNs' antimicrobial machineries are involved in restricting *L. pneumophila* growth within PMNs.

Macrophages respond to infection by various pathogens through immunometabolic reprogramming (56–60), which also occurs in tumors (61). Hyperglycemia in diabetic patients triggers activation of PMNs, similar to *ex vivo* exposure of quiescent PMNs to a high level of glucose (62–64), and this response is mediated through upregulation of aerobic glycolysis (62–65). Similar to the response of macrophages to high levels of glucose through upregulation of aerobic glycolysis, accumulation of lactate, and diminished tricarboxylic acid (TCA) cycle (66–79), PMNs also exhibit upregulation of aerobic glycolysis upon their activation (62–64), and inhibition of glycolysis blocks PMN activation (62). Recent studies have shown that the key glycolytic enzyme 6-phosphofructo-2-kinase (PFK-2) of PMNs interacts with the phagocyte NADPH oxidase (80).

Inhibition of PFK-2 reduces NADPH oxidase activity along with reduced glycolysis, and interference with the NADPH oxidase activity diminishes glycolysis (80). Therefore, there is a unique positive feedback loop between the NADPH oxidase activity and up-regulation of PMNs glycolysis and their activation (80). Interestingly, diabetic patients are more prone to *L. pneumophila* infections (34, 35, 81–83), which may be due to the dysregulated inflammatory response of macrophages and PMNs to persistent high levels of glucose (66–79, 84–86).

Degradation of glycogen/glycogenolysis in mammals is a tightly regulated process to avoid the sudden release of a large amount of intracellular glucose (87). We have recently shown that *L. pneumophila* injects into the cytoplasm of macrophages and the amoeba natural host an amylase (LamA) effector, which rapidly catalyzes rapid unregulated degradation of host glycogen (88). In the natural amoeba host, LamA-mediated glycogenolysis interferes with encystation of amoeba by depriving the natural host of the glucose resource to synthesize the cellulose-rich cyst wall. This renders the amoeba host to remain in the permissive trophozoite form and unable to differentiate into the nonpermissive cyst form (88). In human macrophages, LamA-mediated glycogenolysis generates cytosolic hyperglucose that enhances glycolysis. The macrophages respond by undergoing a paradoxical M1-like proinflammatory response but remain permissive for intracellular survival and replication of *L. pneumophila* (88).

Here, we show that upon injection of LamA into the cytosol of PMNs, the enzyme rapidly degrades the PMNs glycogen, resulting in a cytosolic hyperglucose. The PMNs respond by enhanced glycolysis, which leads to engagement of the two major PMNs bactericidal mechanisms, the robust spatial generation of ROS and fusion of the pathogen-containing phagosomes (LCP) to the specific and azurophilic granules, which collectively restrict the pathogen. Thus, PMNs respond to a functional Dot/Icm system, and injection of LamA in particular, through activation and pathogen restriction, which is counter-evolutionary to pathogen-host adaptation.

RESULTS

Translocation of LamA triggers rapid glycogenolysis in PMNs. Since PMNs possess abundant glycogen stores and are highly glycolytic, we determined if LamA is translocated into PMNs during infection by *L. pneumophila* utilizing strains harboring LamA-adenylate cyclase reporters. At 60 min postinfection, PMNs were lysed, and cAMP levels were measured by enzyme-linked immunosorbent assay (ELISA). The data showed that at 60 min postinfection, wild-type bacteria translocated LamA into the PMNs cytosol similar to the positive-control effector, RaIF, but the *dotA* translocation-deficient mutant ($\Delta T45S$) failed to translocate LamA (Student's *t* test, $P < 0.0001$) (Fig. 1A). When phagocytosis of *L. pneumophila* by PMNs was blocked by cytochalasin D, translocation of LamA was not detected by attached extracellular wild-type bacteria (Fig. 1A), demonstrating that LamA was only translocated into the PMNs' cytosol upon phagocytosis of *L. pneumophila*. Together, this indicates that LamA is rapidly injected into the PMNs' cytosol by the Dot/Icm T45S of intracellular *L. pneumophila*.

To determine the effects of the injected LamA on PMNs glycogen stores in PMNs, glycogen granules were quantified by confocal microscopy using a glycogen-specific antibody. Uninfected PMNs harbored ~30 distinct glycogen granules. At 15 min postinfection, PMNs harboring the wild-type strain contained <10 glycogen granules (Student's *t* test, $P < 0.0001$) (Fig. 1C and D). In contrast, PMNs infected with either the $\Delta lamA$ or $\Delta T45S$ mutants harbored similar numbers of glycogen granules as uninfected PMNs (Fig. 1C and D). Therefore, the injected LamA catalyzes glycogenolysis in PMNs.

To confirm the effects of injected LamA on PMNs on glycogenolysis, we determined the levels of glycogen. The PMNs were infected for 1 h with either the wild type, $\Delta T45S$ or $\Delta lamA$ mutants, the catalytically inactive *lamA/C*^{T99D-A} mutant, the *lamA/C* complemented strain, or formalin-killed wild-type bacteria, and the level of glycogen was determined. As expected, control PMNs that were starved of glucose, glycogen was rapidly depleted within 1 h, indicative of glycogenolysis (Fig. 1B). Strikingly, at 1 h, glycogen was significantly

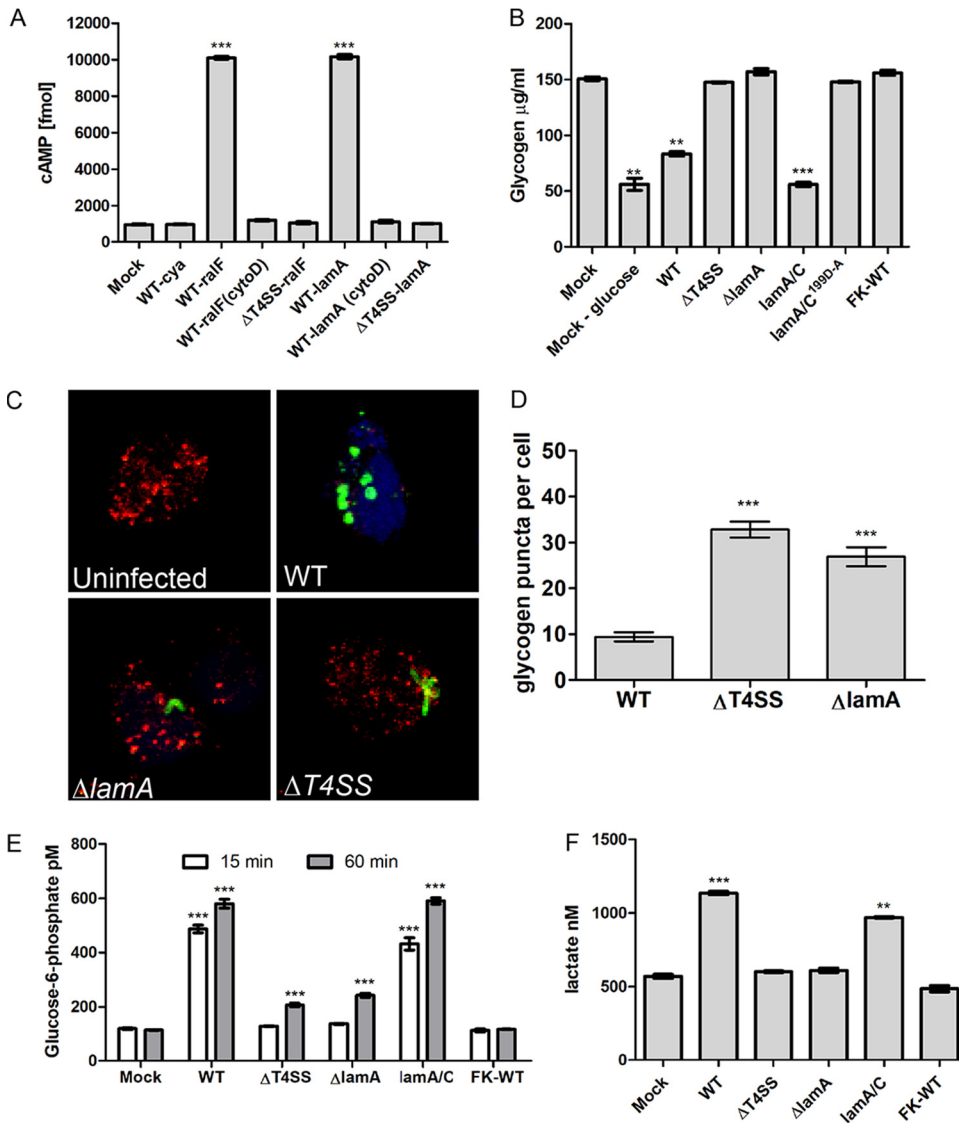


FIG 1 Dot/lcm-injected LamA triggers glycogenolysis in PMNs, resulting in cytosolic hyperglucose and upregulated glycolysis. (A) Adenylate cyclase (Cya) reporter fusion translocation assays of LamA expressed by wild-type *L. pneumophila* and the translocation-deficient $\Delta T4SS$ mutant. The Cya-RalF effector fusion was used as a positive control. PMNs were infected for 1 h in triplicate, and cAMP production was assessed by ELISA. To prevent phagocytosis, cytochalasin D was used. Data are shown as mean cAMP concentration \pm SD, $n=3$. ***, Student's *t* test of WT-RalF or WT-LamA versus WT-Cya; $P < 0.0001$. (B) Quantification of cytosolic glycogen concentrations in PMNs starved of glucose or infected wild type, $\Delta T4SS$, $\Delta lamA$ or *lamA/C* and its catalytically inactive mutant, and formalin-killed wild-type bacteria at 1 h postinfection. Data are shown as mean glycogen concentration \pm SD; $n=3$. **, **, and ***, Student's *t* test of mock minus glucose cells, WT, or *lamA/C* versus mock-treated cells; $P = 0.0037$, $P = 0.0014$, and $P = 0.0007$, respectively. (C) Representative z-stack confocal microscopy images of PMNs infected with various *L. pneumophila* strains (green) and glycogen granules were labeled by antibody (red). (D) Quantification of glycogen granules per cell at 15 min postinfection. Glycogen granules were counted in z-stack confocal images, and data points show mean granules/infected cell \pm SD ($n=100$ infected cells) and are representative of three independent experiments. ***, Student's *t* test of glycogen granules in either $\Delta T4SS$ - or $\Delta lamA$ -infected cells versus wild type-infected cells; $P < 0.0001$. (E) Quantification of cytosolic glucose-6-phosphate levels in PMNs infected with *L. pneumophila* strains at 15 and 60 min postinfection. Data are shown as mean glucose-6-phosphate concentration \pm SD, $n=3$. ***, Student's *t* test of glucose-6-phosphate levels in either wild type- or *lamA/C*-infected cells versus uninfected cells; $P < 0.0001$. (F) Lactate levels in cell culture supernatants of PMNs infected for 1 h with wild type, $\Delta T4SS$, $\Delta lamA$, *lamA/C*, or formalin-killed wild type. Data represent the mean lactate concentration \pm SD, $n=3$. *** and **, Student's *t* test of lactate level in the culture supernatant of wild type or *lamA/C*-infected PMNs versus mock-infected cells; $P < 0.001$ and $P < 0.0013$, respectively. Unless otherwise stated, n represents technical replicates, and data shown are representative of three independent biological replicates.

depleted in PMNs infected by the wild-type strain of *L. pneumophila* compared to mock-infected cells (Student's *t* test, $P < 0.0014$) (Fig. 1B). In contrast, glycogen levels were unaffected in PMNs infected with the $\Delta T4SS$ mutant, the $\Delta lamA$ mutant, the catalytically inactive *lamA* mutant, or the formalin-killed wild type, similar to mock-infected cells (Fig. 1B). Therefore, the catalytic activity of LamA is essential for glycogen degradation in PMNs.

LamA-dependent cytosolic hyperglucose and enhanced glycolysis in PMNs.

Glycogen degradation/glycogenolysis is highly regulated in mammalian cells to prevent a sudden rapid rise in intracellular glucose. To determine if the unregulated and rapid LamA-mediated glycogenolysis in PMNs results in elevation of cytosolic glucose, the level of glucose-6-phosphate (G6P) in infected PMNs was determined. Following 15 min and 60 min infection, G6P levels in wild type- or *lamA/C*-infected PMNs increased ~5-fold compared to mock-infected cells (Student's *t* test, $P < 0.0001$) (Fig. 1E). In contrast, at 15 min, G6P levels in PMNs infected with the $\Delta T4SS$ or $\Delta lamA$ mutants, or formalin-killed wild-type bacteria, were similar to mock-infected cells (Fig. 1E). At 60 min, PMNs infected with the $\Delta T4SS$ or $\Delta lamA$ mutants showed slightly elevated G6P levels compared to mock-infected cells, but the increase was much less than cells infected with the wild type or the complemented *lamA/C* strain (Student's *t* test, $P < 0.0001$) (Fig. 1E).

Since LamA-mediated glycogenolysis in PMNs led to cytosolic hyperglucose, we determined whether PMNs infected by the wild-type bacteria responded to the cytosolic hyperglucose by undergoing immunometabolic reprogramming that involved increased aerobic glycolysis. The PMNs were infected, and the secretion of lactate into the cell culture medium at 1 h postinfection was used as a readout. Infection of PMNs with the wild-type strain resulted in a significant increase in lactate secretion into the cell culture media compared to mock-infected cells (Student's *t* test, $P < 0.001$) (Fig. 1F). In contrast, PMNs infected with the $\Delta T4SS$ or $\Delta lamA$ mutants or formalin-killed wild-type bacteria produced similar amounts of lactate to mock-infected cells (Fig. 1F). Importantly, infection of PMNs with the complemented $\Delta lamA/C$ mutant resulted in increased lactate secretion, similar to infection with the wild-type strain (Fig. 1F). This indicates that in response to LamA-dependent cytosolic hyperglucose, PMNs exhibit immunometabolic reprogramming that involved the hallmark of increased glycolysis.

LamA-dependent rapid degradation of *L. pneumophila* within PMNs.

Permissiveness of human macrophages or the natural amoebal hosts to *L. pneumophila* is totally dependent on a functional Dot/Icm T4SS apparatus since the $\Delta T4SS$ mutant is degraded within macrophages or amoebae. Strikingly, confocal microscopic analyses of *L. pneumophila* morphology revealed that the wild-type bacteria became rounded and fragmented within 15 min of infection (Fig. 1C), while the $\Delta T4SS$ and $\Delta lamA$ mutants remained intact bacillus-shaped bacteria (Fig. 1C). This suggested PMNs actively degraded intracellular wild-type bacteria but not the $\Delta T4SS$ and $\Delta lamA$ mutants. Under the infection conditions, no evidence for neutrophil extracellular traps was observed.

To assess the kinetics of degradation of the wild-type bacteria, PMNs were examined by single-cell analyses using confocal microscopy at 5, 15, and 60 min postinfection. At 5 min postinfection, the morphology of the wild-type strain and both mutants showed no alterations with normal intact bacillus-shaped bacteria. Importantly, the $\Delta T4SS$ and $\Delta lamA$ mutants retained normal bacterial morphology up to 60 min postinfection (Fig. 2A). In contrast, at 15 min, most wild-type bacteria with the functional Dot/Icm T4SS apparatus became rounded and fragmented (Fig. 2A). Viability of the $\Delta lamA$ was compromised, similar to the wild-type strain, when complemented by the native *lamA* gene ($\Delta lamA/C$) but not by the catalytically inactive $\Delta lamA/C^{D199A/E233A/D313A}$ mutants (Fig. S1 in the supplemental material).

To confirm that the wild-type bacteria but not the $\Delta T4SS$ or $\Delta lamA$ mutants were degraded by the PMNs, we examined viability of bacteria by enumerating CFU from infected cells at various time points. At 5 min postinfection, all strains showed similar CFU and are representative of the initial inoculums (Fig. 2B). At 15 and 60 min postinfection, the $\Delta T4SS$ and $\Delta lamA$ mutants showed no reduction in viability (Fig. 2B). In

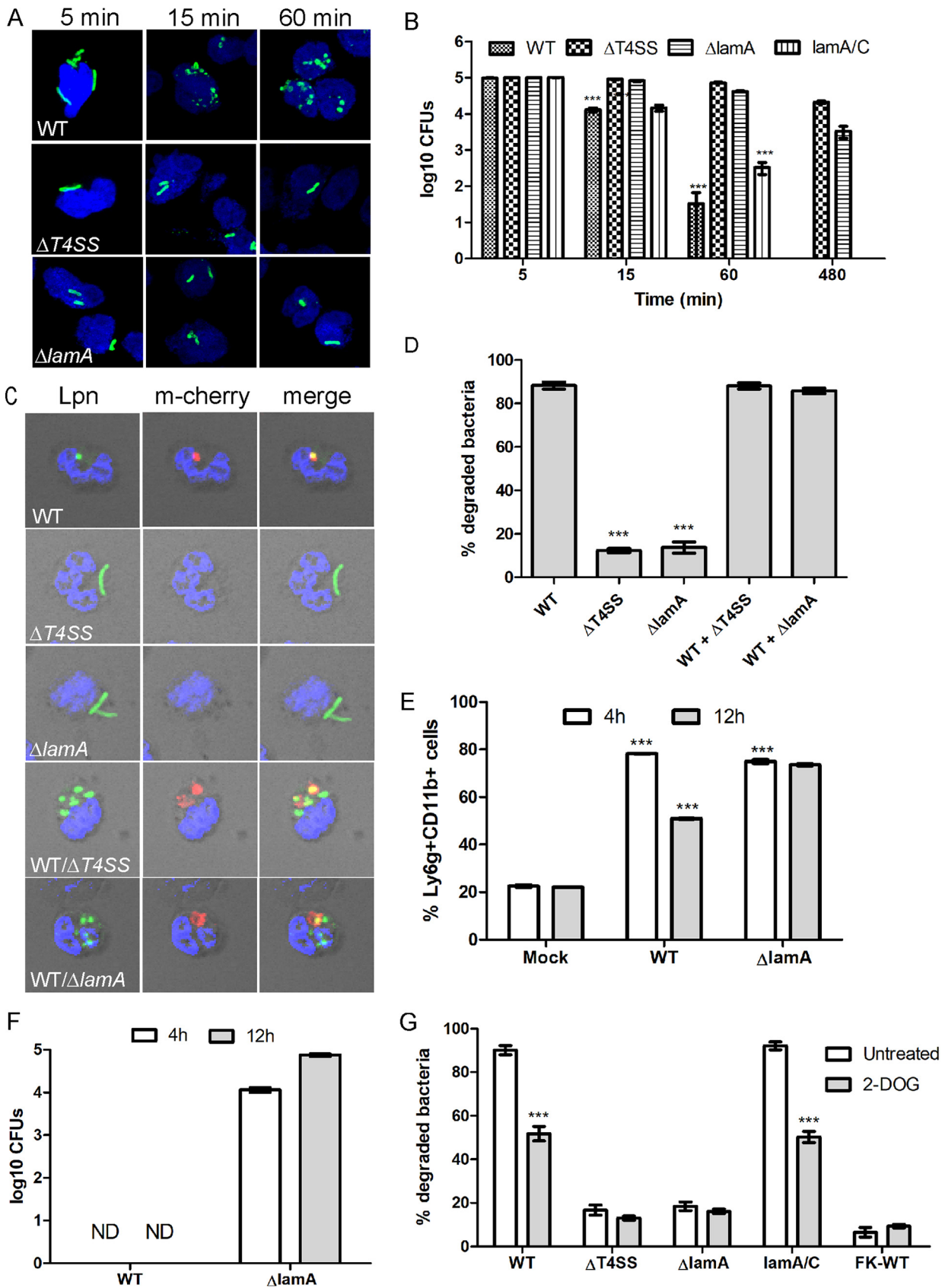


FIG 2 Dot/Lcm- and LamA-dependent rapid killing of *L. pneumophila* by PMNs. (A) Representative confocal images of PMNs infected with either the wild type or the $\Delta T4SS$ or $\Delta lamA$ mutants at 5, 15, and 60 min postinfection. Bacteria are labeled with an anti-*Legionella* antibody (Continued on next page)

addition, the $\Delta T45S$ and $\Delta lamA$ mutants showed little decrease in viable bacteria, even at 8 h postinfection (Fig. 2B). Remarkably, by 15 min postinfection, the wild-type strain and *lamA/C* showed ~ 10 -fold reductions in viability (Student's *t* test, $P < 0.0001$). By 1 h, a further ~ 400 -fold reduction in CFU was observed for the wild-type strain (Student's *t* test, $P < 0.0001$) (Fig. 2B). No viable wild-type strain or *lamA/C* were detected at 8 h postinfection (Fig. 2B).

Previous data have shown that opsonization with both antibody and complement is required for efficient association and uptake of *L. pneumophila* by PMNs (13, 89). Therefore, we determined whether the observed differences in wild-type survival in PMNs compared to the $\Delta T45S$ mutant strain were due to differences in bacterial opsonization and uptake. At 15 min postinfection, uptake of both wild type and the $\Delta T45S$ mutant were similar when opsonized with either fresh human serum or human serum plus anti-*Legionella* antibody (Fig. S2A). Consistent with previous observations, non-opsonized wild-type bacteria were poorly taken up by PMNs at 15 min postinfection, while uptake of nonopsonized $\Delta T45S$ was similar to the opsonized mutant (Fig. S2A). Regardless of opsonization, within 60 min postinfection, both wild-type bacteria and $\Delta T45S$ mutant bacteria were taken up by PMNs at similar levels (Fig. S2A). Although formalin-killed bacteria generally showed lower uptake by PMNs compared to wild-type and $\Delta T45S$ mutant bacteria, there was no statistically significant difference (Fig. S2A).

Next, we examined if bacterial degradation was altered by opsonization. The data showed that the majority of wild-type bacteria opsonized with human serum or human serum plus anti-*Legionella* antibody were degraded at 15 min postinfection, while most $\Delta T45S$ mutant bacteria remained intact (Fig. 2B). At 60 min postinfection, there was an increase in degradation of the $\Delta T45S$ mutant bacteria, but this was not statistically significant. As expected, minimal degradation of formalin-killed wild-type bacteria was observed at 15 and 60 min postinfection regardless of opsonization (Fig. 2B). We conclude that both opsonized wild-type and $\Delta T45S$ bacteria were taken up similarly by PMNs (Fig. 2A), and the degradation of wild-type bacteria is not due to differences in uptake and opsonization compared to the $\Delta T45S$ mutant bacteria. Thus, in contrast to the Dot/Icm-dependent permissiveness of macrophages to *L. pneumophila*, PMNs rapidly degrade wild-type *L. pneumophila* in a Dot/Icm-dependent manner, and specifically, the LamA effector is essential for rapid restriction of *L. pneumophila* by PMNs.

Next, we determined if cohabitation of wild-type bacteria with the $\Delta T45S$ or $\Delta lamA$ mutants within the same PMN resulted in rapid killing of the mutants. To achieve this, PMNs were infected with either the wild type expressing mCherry or the $\Delta T45S$ and $\Delta lamA$ mutants individually or coinfecting with the wild type expressing mCherry and the $\Delta T45S$ or $\Delta lamA$ mutants together. Following 1 h infection, bacterial morphology in infected PMNs was examined by confocal microscopy (Fig. 2C and D). In PMNs infected with wild-type bacteria alone, $\sim 90\%$ of bacteria showed deformed morphology, while only 12% and 14% of $\Delta T45S$ or $\Delta lamA$ bacteria showed deformed morphology (Fig. 2C and D). In contrast, in PMNs coinfecting with both wild type and the $\Delta T45S$

FIG 2 Legend (Continued)

(green), and nuclei are stained with DAPI (blue). (B) Survival of *L. pneumophila* in PMNs was determined by measuring recoverable CFU from infected cells. PMNs were infected with the wild type or the $\Delta T45S$ or $\Delta lamA$ mutants or the complemented *lamA/C* mutant, and CFU were determined at 5, 15, 60, and 480 min postinfection. Data are shown as mean \log_{10} CFU \pm SD; $n = 3$. ***, Student's *t* test CFU at 15 and 60 min relative to 5 min; $P < 0.0001$. (C and D) Degradation of the $\Delta T45S$ or $\Delta lamA$ mutants in PMNs when cohabiting the same cell with wild-type bacteria. PMNs were infected with the wild type expressing mCherry alone (red), the $\Delta T45S$ or $\Delta lamA$ mutants alone, or with wild type coinfecting with $\Delta T45S$ or $\Delta lamA$ mutants. Following 1 h infection, bacterial morphology was examined by confocal microscopy. Representative confocal images are shown in panel C and quantification in panel D. Data are shown as mean percent degraded bacteria \pm SD; $n = 100$, ***, Student's *t* test of percent degraded $\Delta T45S$ or $\Delta lamA$ mutants in PMNs versus wild-type bacterial cells; $P < 0.0001$. (E) Analysis of Ly6g⁺ CD11b⁺ PMN infiltration in lungs of mock-infected mice or infected with either the wild type or $\Delta lamA$ mutant at 4 h and 12 h postinfection. (F) Survival of the wild type or the $\Delta lamA$ mutant in Ly6g⁺ CD11b⁺ PMNs isolated from the lungs of infected mice. (G) Survival of *L. pneumophila* in PMNs during inhibition of glycolysis with 2-deoxyglucose was determined by confocal microscopy. PMNs pretreated with 2-deoxyglucose were infected with wild type or the $\Delta T45S$ or $\Delta lamA$ mutants or formalin-killed wild type, and bacterial morphology was examined at 15 min postinfection. ***, Student's *t* test of percent degraded wild type or *lamA/C* bacteria in PMNs treated with 2-deoxyglucose versus untreated cells; $P < 0.0001$. Unless otherwise stated, *n* represents technical replicates, and data shown are representative of three independent biological replicates.

or $\Delta lamA$ mutants, 90% of all bacteria exhibited deformed morphology (Student's *t* test, $P < 0.0001$) (Fig. 2C and D). This indicates that, in response to injection of LamA by wild-type bacteria, PMNs are activated and restrict the coinhabiting $\Delta T45S$ or $\Delta lamA$ mutants.

To confirm the LamA-dependent rapid killing of *L. pneumophila* by PMNs in an *in vivo* infection model, A/J mice were infected with either the wild-type strain or the $\Delta lamA$ mutant and PMNs collected at 4 h and 12 h postinfection by bronchoalveolar lavage (BAL) fluid. At 4 h and 12 h postinfection, BAL fluid was retrieved from infected mice and analyzed by flow cytometry to determine the PMN Ly6g-positive (Ly6g⁺) CD11b⁺ cell population. The data showed a dramatic influx of Ly6g⁺ CD11b⁺ cells at 4 h in both wild-type and $\Delta lamA$ -infected mice compared to mock-infected mice (Student's *t* test, $P < 0.0001$) (Fig. 2E). At 12 h postinfection, the number of Ly6g⁺ CD11b⁺ cells fell to 50% in wild type-infected mice (Student's *t* test, $P < 0.0001$), but no reduction was seen in $\Delta lamA$ -infected mice (Fig. 2E). Next, we determined recoverable bacterial CFU in the PMNs sorted from the BAL fluid. In wild type-infected mice, no recoverable CFU were obtained in the Ly6g⁺ CD11b⁺ PMNs population. In contrast, ~ 4 - to 5 -log₁₀ CFU of the $\Delta lamA$ mutant were recovered from the sorted PMNs (Fig. 2F). This indicates that similar to *ex vivo* in human PMNs, wild-type bacteria are rapidly cleared by PMNs *in vivo*, and this killing is LamA dependent.

Enhanced glycolysis-mediated activation of PMNs in response to cytosolic hyperglucose. We examined if increased glycolysis in response to LamA-dependent cytosolic hyperglucose resulted in PMNs activation and rapid killing of *L. pneumophila*. The PMNs were pretreated with the glycolysis inhibitor 2-deoxyglucose (2-DOG), and infected and bacterial morphology were examined by confocal microscopy. Prolonged exposure to 2-DOG is toxic to *L. pneumophila* (90), but the 15 min exposure of *L. pneumophila* to this inhibitor did not impair viability (Fig. S3). In mock-infected PMNs, $\sim 90\%$ of wild-type bacteria exhibited deformed morphology. However, in PMNs where glycolysis was inhibited, only $\sim 50\%$ of wild-type bacteria showed deformed morphology (Student's *t* test, $P < 0.0001$) (Fig. 2G). In PMNs infected with the $\Delta T45S$ or $\Delta lamA$ mutants or formalin-killed wild-type bacteria, most bacteria maintained normal morphology, and inhibition of glycolysis did not impact this (Fig. 2G). Importantly, PMNs infected with the complemented *lamA/C* mutant, $\sim 90\%$ of the bacteria exhibited deformed morphology, but in PMNs where glycolysis was inhibited, only $\sim 50\%$ showed deformed morphology (Student's *t* test, $P < 0.0001$) (Fig. 2G). This indicates that PMNs respond to cytosolic hyperglucose generated by LamA-dependent glycolysis and increased glycolysis leading to activation of PMNs and restriction of *L. pneumophila*.

Spatial ROS production by PMNs within the LCP. One of the two major antimicrobial arms of the PMN response to bacterial infection is the oxygen-dependent generation of ROS by the phagocyte NADPH oxidase. Since *L. pneumophila* was rapidly killed by PMNs, we determined if PMNs generated intracellular ROS (icROS) in response to *L. pneumophila* infection (91). Control PMNs were stimulated with PMA or zymosan as a positive control for icROS production. The data showed that in response to infection with the wild-type strain or the complemented *lamA/C* mutant, PMNs produced significantly more icROS (Student's *t* test, $P = 0.0104$ and $= 0.0058$, respectively) than cells infected with the $\Delta T45S$ or $\Delta lamA$ mutants or formalin-killed wild-type bacteria (Fig. 3A).

To determine if the increased icROS production in PMNs occurred spatially within the LCP, PMNs were stained using nitroblue tetrazolium (NBT), which forms dense deposits in the presence of ROS. The data showed that phagosomes harboring either the wild-type strain or the complemented *lamA/C* mutant colocalized with dense deposits of NBT, but little or no NBT staining was seen in PMNs infected with the $\Delta T45S$ or $\Delta lamA$ mutants or formalin-killed wild-type bacteria (Fig. 3B). Importantly, NBT staining was spatial and limited subcellularly to the LCP (Fig. 3B).

Since ROS was spatially generated within the wild-type (WT) strain LCP, we determined if ROS contributes to the rapid killing of wild-type bacteria. To determine this,

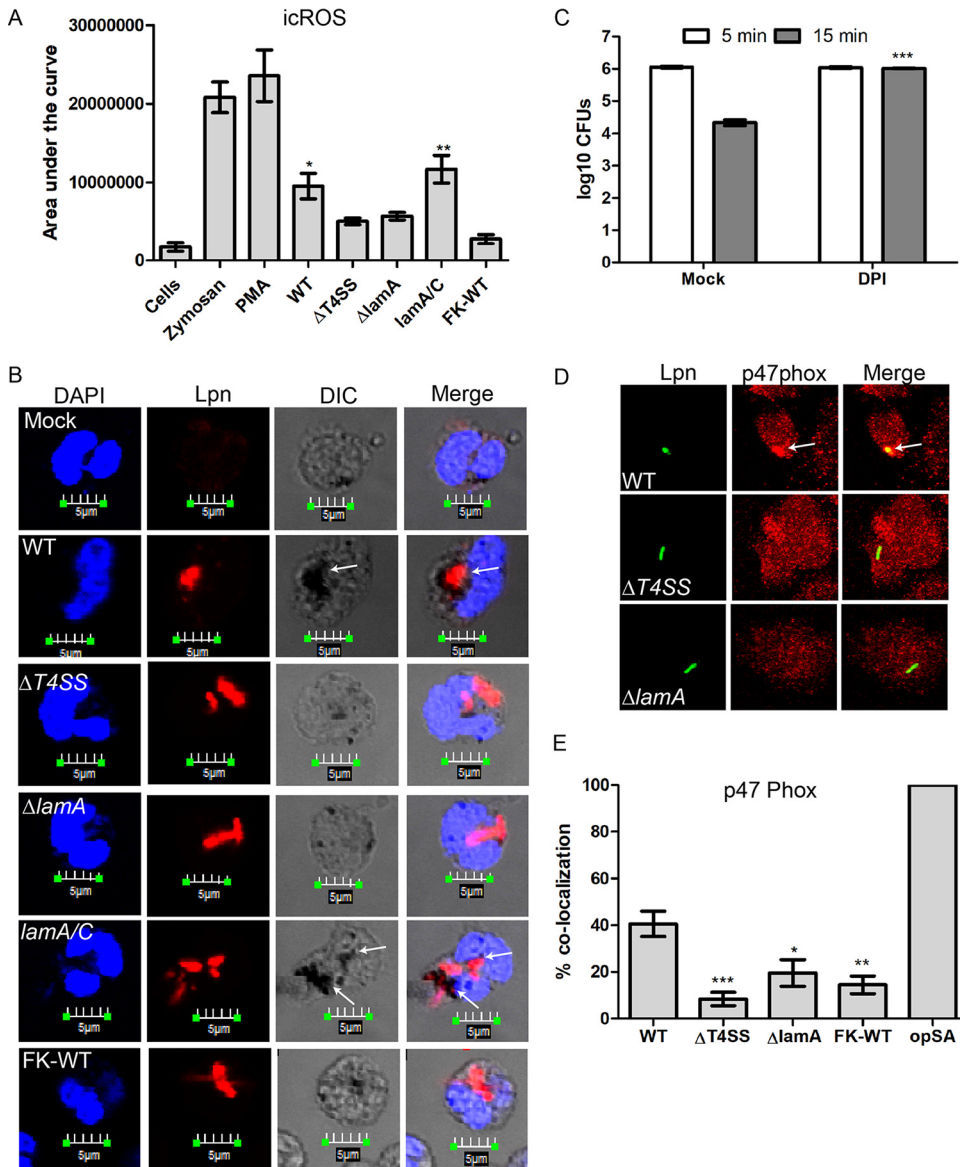


FIG 3 Generation of a robust ROS burst by PMNs in response to cytosolic hyperglucose generated by LamA-mediated glycogenolysis. (A) Determination of ROS produced by PMNs in response to *L. pneumophila* infection. PMNs were infected with either the wild-type bacteria or the $\Delta T4SS$ and $\Delta lamA$ mutants, the complemented *lamA/C* mutant, or formalin-killed wild type for 1 h. Additionally, PMNs were stimulated with zymosan or PMA as a positive control for ROS production. *, Student's *t* test of ROS production by PMNs infected with either $\Delta T4SS$ or the $\Delta lamA$ mutant versus wild type infected PMNs; $P = 0.0277$, 0.0432 , respectively. (B) Representative confocal microscopy images showing spatial subcellular localization of ROS production in the pathogen containing phagosome. PMNs treated with NBT were infected with wild type or the $\Delta T4SS$ or $\Delta lamA$ mutants, the complement *lamA/C* mutant, or formalin-killed wild type for 1 h. Bacteria were stained using an anti-*L. pneumophila* antibody (red), and nuclei were stained with DAPI (blue). NBT staining is shown in differential interference contrast (DIC) images as black deposits. (C) The contribution of ROS to rapid bacterial killing was determined using the inhibitor DPI. PMNs were pretreated with DPI and infected with wild-type bacteria, and recoverable CFU were determined at 5 and 15 min postinfection. Data are shown as mean \log_{10} CFU \pm SD; $n = 3$. ***, Student's *t* test of wild-type CFU in DPI-treated PMNs at 15 min versus untreated PMNs; $P < 0.0001$. (D) Representative confocal images showing spatial subcellular colocalization of p47phox with the *L. pneumophila* phagosome. PMNs were infected with wild type or the $\Delta T4SS$ or $\Delta lamA$ mutants for 15 min. Bacteria are stained with an anti-*Legionella* antibody (green), and p47phox is stained with anti-p47phox (red). (E) Quantification of p47phox colocalization to the pathogen-containing phagosome at 15 min postinfection. Data are shown as mean percent colocalization \pm SD; $n = 100$. ***, *, and **, Student's *t* test of percent colocalization of p47phox to phagosomes harboring the $\Delta T4SS$ or $\Delta lamA$ mutants, formalin-killed wild type, or opsonized *S. aureus* versus wild type containing phagosomes; $P = 0.0008$, $= 0.0288$, and $= 0.0043$, respectively. Unless otherwise stated, *n* represents technical replicates, and data shown are representative of three independent biological replicates.

PMNs were pretreated with the ROS inhibitor diphenyleneiodonium (DPI) prior to infection, and recoverable bacterial CFU were enumerated. At 5 min postinfection, similar numbers of CFU were recovered from mock- and DPI-treated PMNs (Fig. 3C). However, at 15 min, ~100-fold fewer wild-type bacteria were recovered from mock-treated PMNs (Fig. 3C). In contrast, in DPI-treated PMNs, no significant reduction in recoverable CFU was observed (Student's *t* test, $P < 0.0001$) (Fig. 3C). Our data indicate that spatial generation of ROS within LCP plays a key role in the rapid killing of wild-type bacteria in PMNs.

Acquisition of the phagocyte NADPH oxidase by the LCP. Since PMNs produced increased ROS in response to wild-type strain infection and this ROS is spatially produced within the LCP, we examined recruitment of the NADPH oxidase cytosolic component p47phox to the LCP at 5, 15, and 60 min postinfection (Fig. 3D and E; Fig. S4A). Opsonized *Staphylococcus aureus* was used as a positive control for recruitment of the NADPH oxidase. As early as 5 min postinfection, ~33% of wild-type LCPs colocalized with p47phox (Fig. S4A), while LCPs harboring the $\Delta T45S$ or $\Delta lamA$ mutants or formalin-killed wild-type bacteria showed significantly less colocalization with p47phox (Fig. S4A). At 15 min postinfection, ~40% of wild-type LCPs colocalized with p47phox (Fig. 3D and E). In contrast, ~20% or fewer phagosomes harboring the $\Delta T45S$ or $\Delta lamA$ mutants, or formalin-killed wild-type bacteria colocalized with p47phox (Student's *t* test, $P < 0.0008$, $P < 0.0288$, and $P < 0.0043$, respectively) (Fig. 3D and E). Following 1 h of infection, localization of p47phox to wild-type LCPs increased to ~50%, while LCPs harboring the $\Delta T45S$ or $\Delta lamA$ mutants, or formalin-killed wild-type bacteria, were still below 20% (Student's *t* test, $P < 0.0001$) (Fig. S4A). Taken together, these indicate that the phagocyte NADPH oxidase complex is spatially targeted to the wild-type strain containing phagosomes in a Dot/Icm- and LamA-dependent manner.

LamA-dependent fusion of neutrophil granules to the LCP. The other major arm of the PMNs microbicidal activity is the fusion of specific and azurophilic granules to bacteria-containing phagosomes. Therefore, we determined whether the antimicrobial matrix contents of specific and azurophilic granules were delivered to the LCP. Within 5 min, ~40% of wild type containing phagosomes colocalized with lactoferrin and elastase, markers for specific and azurophilic granules, respectively, similar to the opsonized *S. aureus* control (Fig. S4B and C). In contrast, less than 10% of phagosomes containing either the $\Delta T45S$ or $\Delta lamA$ mutants or formalin-killed wild-type bacteria colocalized to either lactoferrin or elastase (Student's *t* test, $P < 0.0001$) (Fig. S4B and C).

At 15 min postinfection, ~40% of wild-type LCPs still colocalized with lactoferrin, but colocalization with elastase increased to ~60%, similar to the opsonized *S. aureus* control, while less than 15% of phagosomes containing either the $\Delta T45S$ or $\Delta lamA$ mutants or formalin-killed wild-type bacteria colocalized to either lactoferrin or elastase (Student's *t* test, $P < 0.0001$) (Fig. 4A to D). At 1 h postinfection, colocalization of lactoferrin with phagosomes harboring wild-type bacteria diminished to ~24% compared to ~44% for the opsonized *S. aureus* control (Fig. S4B). However, colocalization of lactoferrin to LCPs containing the $\Delta T45S$ or $\Delta lamA$ mutants, or formalin-killed wild-type bacteria, was still lower than that observed for wild type containing phagosomes but not statistically significant (Fig. S4B). In contrast, at 1 h postinfection, 67% of LCPs harboring the wild-type strain still colocalized with elastase, similar to the opsonized *S. aureus* control (Fig. S4C). However, LCPs containing either the $\Delta T45S$ or $\Delta lamA$ mutants or formalin-killed wild-type bacteria still showed significantly lower colocalization with elastase than the wild-type strain (Student's *t* test, $P < 0.0001$) (Fig. S4C).

Since both specific and azurophilic granules fused to the wild type containing LCPs, we determined if these granules contribute to the rapid killing of wild-type bacteria in addition to ROS. To determine this, PMNs were either pretreated with a pan-protease inhibitor, a cathepsin G inhibitor (specific granules), or an elastase inhibitor (azurophilic granules) and infected with wild-type bacteria for 5 and 15 min, and recoverable CFU were enumerated. At 5 min postinfection, similar numbers of wild-type CFU were recovered from PMNs treated with the inhibitors compared to mock-treated cells (Fig. 4E). At 15 min postinfection, recoverable CFU were reduced by ~100-fold in

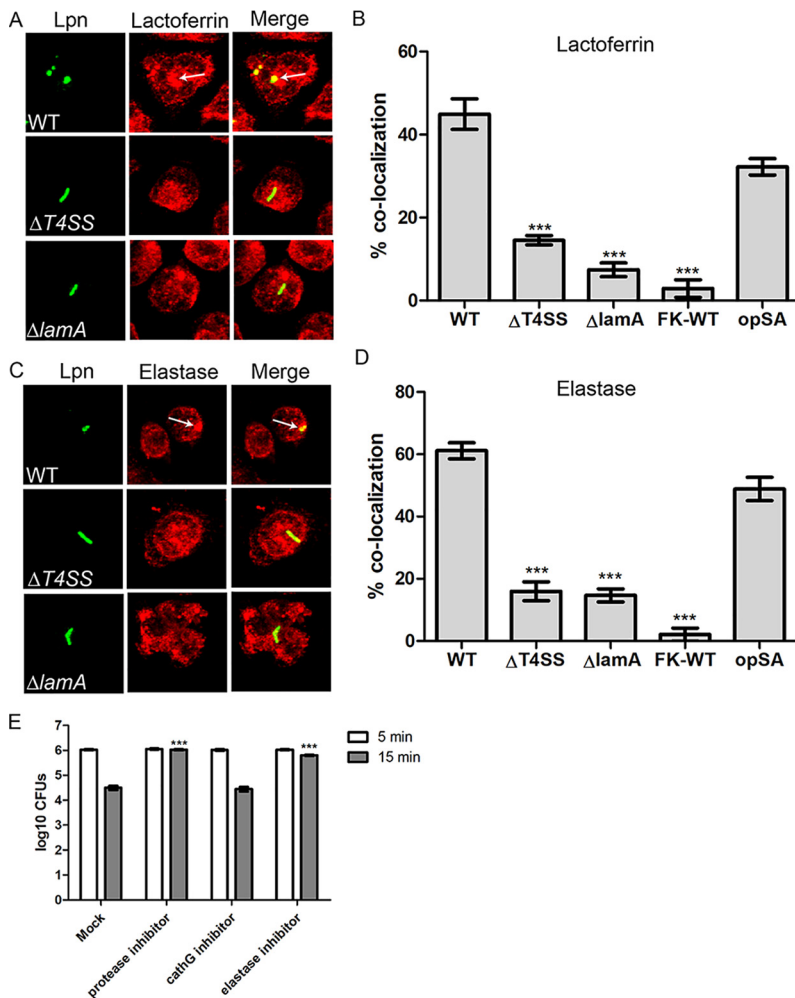


FIG 4 LamA-dependent fusion of specific and azurophilic granules to the *L. pneumophila* phagosome. (A) Representative confocal images showing colocalization of lactoferrin with the *L. pneumophila* phagosome. PMNs were infected with wild type or the $\Delta T4SS$ or $\Delta lamA$ mutants, formalin-killed wild type, or opsonized *S. aureus* for 15 min. Bacteria are stained with an anti-*Legionella* antibody (green), and lactoferrin is stained with anti-lactoferrin (red). (B) Quantification of lactoferrin colocalization to the *L. pneumophila* phagosome at 15 min postinfection. Data are shown as mean percent colocalization \pm SD; $n=100$. ***, Student's *t* test of percent colocalization of lactoferrin to phagosomes harboring the $\Delta T4SS$ or $\Delta lamA$ mutants or formalin-killed wild type versus wild type containing phagosomes; $P<0.0001$. (C) Representative confocal images showing colocalization of elastase with the *L. pneumophila* phagosome. PMNs were infected with wild type or the $\Delta T4SS$ or $\Delta lamA$ mutants, formalin-killed wild type, or opsonized *S. aureus* for 15 min. Bacteria were labeled with an anti-*Legionella* antibody (green), and elastase is labeled with anti-elastase antibodies (red). (D) Quantification of elastase colocalization to the *L. pneumophila* phagosome at 15 min postinfection. Data are shown as mean percent colocalization \pm SD; $n=100$. ***, Student's *t* test of percent colocalization of elastase to phagosomes harboring the $\Delta T4SS$ or $\Delta lamA$ mutants or formalin-killed wild type versus wild type containing phagosomes; $P<0.0001$. (E) Relative contribution of specific and azurophilic granules to rapid bacterial killing was determined using a pan-protease, cathepsin G, and elastase inhibitors. PMNs were pretreated with DPI and infected with wild-type bacteria, and recoverable CFU were determined at 5 and 15 min postinfection. Data are shown as mean \log_{10} CFU \pm SD; $n=3$. ***, Student's *t* test of wild-type CFU in PMNs treated with the pan-protease or elastase inhibitors at 15 min versus untreated PMNs; $P<0.0001$. Unless otherwise stated, n represents technical replicates, and data shown are representative of three independent biological replicates.

mock-treated PMNs. In contrast, in PMNs treated with the pan-protease inhibitor or the elastase inhibitor, wild-type bacterial viability was not altered at 15 min postinfection (Student's *t* test, $P<0.0001$) (Fig. 4E). In PMNs treated with the cathepsin G inhibitor, recoverable wild-type CFU were similar to mock-treated cells (Fig. 4E), indicating that blocking specific granules had little or no effect on the ability of PMNs to restrict wild-type

bacteria. Taken together, fusion of azurophilic granules to the LCP along with spatial ROS generation within the LCP contribute to the rapid restriction of *L. pneumophila*. Pathogen restriction is dependent on immunometabolic reprogramming and activation of the PMNs in response to cytosolic hyperglucose generated by rapid and uncontrolled LamA-mediated unregulated glycogenolysis.

DISCUSSION

PMNs represent key immune cells in the innate defense against bacterial pathogens. Many human intracellular bacterial pathogens have undergone selective evolutionary pressure and adaptation to the hosts they invade to interfere with the inflammatory response and innate defenses of macrophages and PMNs to override pathogen restriction in these phagocytic cells (92, 93). In contrast to the general theme of pathogens being specialists in terms of their host range, *L. pneumophila* is a generalist that resides in a diverse range of amoebae species in the environment and has acquired a large repertoire of effector proteins to survive and proliferate within these host cells (6). Indeed, deletion of one-third of the known *L. pneumophila* effectors does not impact the ability of *L. pneumophila* to replicate in mouse-derived macrophages (94). It is thought that the large arsenal of *L. pneumophila* effectors with an unusually high level of redundancy represents a toolbox for adaptation to various environmental hosts (6). Even though *L. pneumophila* can infect and proliferate in human macrophages, causing an accidental pneumonia, this bacterial pathogen has not evolved strategies to effectively overcome the mammalian innate immune response of PMNs. In 1981, it was reported that PMNs restrict *L. pneumophila*, but the mechanisms remained unknown (55), even 40 years later. Here, we show that human PMNs rapidly kill *L. pneumophila*. The mechanism is mediated by the PMNs' direct response to the cellular and biochemical effects of LamA injection through the Dot/Icm type IV secretion system. The injected LamA enzyme catalyzes rapid unregulated glycogenolysis, leading to a sudden cytosolic hyperglucose that upregulates glycolysis, which triggers PMNs activation. Paradoxically, the LamA effector results in rapid activation of PMNs, leading to *L. pneumophila* degradation by the PMNs' two major bactericidal machineries, which are the spatial generation of ROS within the LCV, and fusion of azurophilic and specific granules to the phagosome, which effectively degrade *L. pneumophila* within 15 to 60 min postphagocytosis.

The LamA-dependent activation of PMNs may mimic hyperglycemia in diabetic patients. Hyperglycemia triggers activation of PMNs similar to *ex vivo* exposure of quiescent PMNs to high glucose (62–64), and this response is mediated through upregulation of aerobic glycolysis (62–64). However, unlike hyperglycemia, which is limited by the bottleneck of glucose uptake by the glucose transporter, LamA-mediated glycogenolysis results in an ~5- to 6-fold rise in cytosolic glucose-6-phosphate levels. It is possible that the elevated glucose-6-phosphate levels in PMNs infected with wild-type bacteria come from both the elevated glycogenolysis observed and through increased transport of extracellular glucose. However, this is unlikely since our previous study (88) has demonstrated that the rapid rise in intracellular glucose-6-phosphate came directly from elevated glycogenolysis and not increased transport of extracellular glucose since blocking GLUT1 transport had no effect on the rapid rise of glucose levels. Due to the bottleneck of limited glucose import by the glucose transporters in the plasma membrane, this level of LamA-generated cytosolic glucose is not achieved even in severe cases of chronic hyperglycemia. This may trigger other dysregulated immunometabolic changes that impact killing of *L. pneumophila* (95). Although LamA performs the same catalytic activity in both human macrophages (88) and PMNs, the outcome of unregulated glycogenolysis is different since macrophages are permissive, while PMNs restrict and degrade *L. pneumophila*.

Since the type IV translocation deficient mutant survived in PMNs better than the *lamA* mutant, it is likely that effectors other than LamA also contribute to the ability of human PMNs to sense and then rapidly kill *L. pneumophila*. Furthermore, formalin- or

heat-killed *L. pneumophila* appeared to be resistant to degradation by PMNs, which may be attributable to the inert nature of *L. pneumophila* LPS (96), suggesting multiple factors besides LamA contribute to the ability of human PMNs to sense and kill this pathogen, but the other mechanisms behind this remain to be elucidated.

The coevolution of *L. pneumophila* with its amoebal hosts has equipped this bacteria with a large and redundant arsenal of effectors to survive in these diverse and hostile hosts (6). Many of the effectors in the *L. pneumophila* molecular toolbox are likely specific to certain environmental hosts and are either dispensable in other hosts or have paradoxical consequences. For example, LamA is required to subvert amoebal encystation to enhance its survival in the environmental host, but in human macrophages, this effector promotes a proinflammatory response that partially restricts *L. pneumophila* replication (88). Even though not all effectors are required for survival in host cells, the Dot/Icm translocation system itself is essential for *L. pneumophila* survival in amoebae and human macrophages and therefore represents the key virulence system of this pathogen. However, when *L. pneumophila* encounters mammalian PMNs in the accidental dead-end human host, it is ill-equipped to subvert killing. In contrast to amoebae and macrophages, the Dot/Icm translocation system and the associated cadre of effectors injected into the host cells and, in particular, LamA, may represent an unintended antivirulence process for *L. pneumophila* in PMNs through triggering the two major microbicidal arms of the innate defense of PMNs. The accidental LamA-dependent hyperglucose in PMNs is responsible for their activation and rapid degradation of *L. pneumophila* by PMNs. These findings highlight unexpected phenotypes of amoebae-adapted effectors of *L. pneumophila* that have evolved to interfere with processes of the amoeba natural host with unintended paradoxical effects in the accidental human host.

MATERIALS AND METHODS

Strains and cell lines. *L. pneumophila* strain AA100/130b (ATCC BAA-74), the T4SS-deficient mutant ($\Delta T4SS$), $\Delta lamA$, the complemented *lamA/C*, and the catalytically inactive mutant *lamA/C*^{199D-A} were grown on BCYE agar. For infections, bacteria were grown overnight to post-exponential phase in BYE broth culture to an optical density at 550 nm (OD₅₅₀) of 2 to 2.2. Neutrophils were isolated from venous blood of healthy donors using plasma-Percoll gradients (91). Recruitment of donors, as well as the blood draws, was in accordance with the guidelines approved by the institutional review board of the University of Louisville. Isolated cells showed that ≥ 90 to 95% were neutrophils by microscopic evaluation of cytospins and Wright staining. Trypan blue exclusion indicated that $>97\%$ of cells were viable.

Opsonization of *L. pneumophila* for PMN infection. For infection of PMNs, *L. pneumophila* was opsonized. A total of 500 μ l of post-exponential-phase *L. pneumophila* broth culture was pelleted by centrifugation and resuspended in 500 μ l of sterile water. A total of 1×10^8 bacteria were added to 500 μ l of Hanks buffered salt solution (HBSS) containing 10% pooled human serum and 1 μ l of mouse anti-*Legionella* monoclonal antibody. Following 30 min incubation at room temperature, opsonized bacteria were pelleted by centrifugation and resuspended in 100 μ l sterile water. For some experiments, *L. pneumophila* was killed using 4% (vol/vol) formaldehyde prior to opsonization. Briefly, post-exponential-phase bacteria were pelleted by centrifugation and resuspended in water containing 4% (vol/vol) formaldehyde and incubated at room temperature for 30 min. Bacteria were then washed three times with sterile water prior to opsonization.

Translocation assay. To assess translocation of LamA by *L. pneumophila* during infection of PMNs, an adenylate cyclase fusion to the N terminus of LamA (97) was used as described previously. A total of 10×10^6 PMNs were infected with wild-type or $\Delta T4SS$ mutant *L. pneumophila* harboring plasmids expressing various adenylate cyclase fusions at a multiplicity of infection (MOI) of 1 for 1 h as described previously (97, 98). In some wells, to prevent phagocytosis, PMNs were pretreated with cytochalasin D prior to infection. Following infection, the cell monolayers were lysed and processed to assess cAMP concentration by ELISA using the Direct cAMP ELISA kit (Enzo) according to the manufacturer's instructions.

Analysis of intracellular glycogen. Glycogen levels in human monocyte-derived macrophages (hMDMs) during infection by *L. pneumophila* were determined using the EnzyChrom glycogen assay kit (Bioassay Systems). Briefly, a total of 10×10^6 PMNs were seeded into 6-well plates and infected with the wild type, $\Delta T4SS$, $\Delta lamA$, *lamA/C*, the catalytically inactive mutant, or formalin-killed wild type at an MOI of 1 for 1 h. As a control for glycogenolysis, PMNs were starved of glucose throughout the experiment. Cells were harvested and lysed in 25 mM sodium citrate containing 60 mM NaF (99). Following centrifugation at $13,000 \times g$ for 5 min to pellet cellular debris, the supernatants were then analyzed following the manufacturers' instructions. Degradation of intracellular glycogen was also determined using confocal microscopy. To achieve this, PMNs were plated into 24-well plates containing glass coverslips (3×10^6 cells per well) and infected with either post-exponential-phase wild type or the $\Delta T4SS$ and

$\Delta lamA$ mutants at an MOI of 1. At 15 min postinfection, the monolayers were fixed with 4% formaldehyde for 30 min and permeabilized with 0.1% Triton X-100 in phosphate-buffered saline (PBS) for 15 min. The monolayers were labeled with rabbit anti-*Legionella* antiserum (1:1,000 dilution); mouse anti-glycogen antibody (ESG1A9mAB, 1:50 dilution) (100), a kind gift from Ashida (Kobe University); and counterlabeled with Alexa Fluor 488 anti-rabbit IgG antibody and Alexa Fluor 594 anti-mouse IgM (1:4,000 dilution, Invitrogen) and 4',6-diamidino-2-phenylindole (DAPI) to stain nuclei. The cells were examined by confocal microscopy using an Olympus FV1000 laser scanning confocal microscope (Olympus). Quantification of glycogen granules was performed manually by counting z-stack images (8 μ M depth with 0.2 μ M slices) of infected cells. Over 100 infected cells were counted for each condition and performed in triplicate.

Determination of cytosolic glucose-6-phosphate. To determine G6P levels in infected PMNs of 10×10^6 cells were infected with either wild type, $\Delta T4SS$, $\Delta lamA$, the complemented *lamA/C* or formalin-killed wild-type bacteria at an MOI of 1 for 15 or 60 min. Following infection, the infected cells were collected in ice-cold PBS and rapidly homogenized on ice. Samples were centrifuged (16,000 $\times g$ for 20 min at 4°C), and the resulting supernatants were subjected to deproteinization using a deproteinizing sample preparation kit (BioVision) following the manufacturer's instructions (101–103). The samples were analyzed for G6P using a high-sensitivity glucose-6-phosphate assay kit (Sigma), according to the manufacturer's instructions, with a Synergy H1 microplate reader (Biotek).

Determination of secreted lactate by infected PMNs. To determine lactate secretion by infected PMNs into the culture medium, a total of 10×10^6 PMNs in triplicate were infected with either wild type, $\Delta T4SS$, $\Delta lamA$, the complemented *lamA/C*, or formalin-killed wild-type bacteria at an MOI of 1 for 1 h. Following infection, the culture medium was retained and cooled on ice and subjected to deproteinization using a deproteinizing sample preparation kit (BioVision) following the manufacturer's instructions (104, 105). The samples were analyzed for lactate using a lactate assay kit (Sigma) according to the manufacturer's instructions with a Synergy H1 microplate reader (Biotek).

Determination of bacterial killing by PMNs. To determine killing of *L. pneumophila* during infection of PMNs, infections were initially monitored by confocal microscopy. To achieve this, PMNs were plated into 24-well plates containing glass coverslips (3×10^6 cells per well) and infected with either post-exponential-phase wild type or the $\Delta T4SS$ and $\Delta lamA$ mutants at an MOI of 1. At 5, 15, and 60 min postinfection, the monolayers were fixed with 4% formaldehyde for 30 min and permeabilized with 0.1% Triton X-100 in PBS for 15 min. The monolayers were labeled with rabbit anti-*Legionella* antiserum (1:1,000 dilution), and intracellular bacterial morphology was analyzed by confocal microscopy. In some experiments, PMNs were coinfecting with wild-type bacteria expressing mCherry with either the $\Delta T4SS$ or $\Delta lamA$ mutants. To determine if irregular bacterial morphology correlated with bacterial killing by PMNs, recoverable CFU were determined. A total of 2×10^6 PMNs in triplicate were seeded into 24-well plates and infected with the wild type, $\Delta T4SS$, $\Delta lamA$, or the complemented *lamA/C* mutant at an MOI of 1. At 5, 15, 60, and 480 min postinfection, the culture supernatant was removed, and PMNs monolayers were lysed with sterile water. Bacterial CFU were determined by plating serial dilutions of the PMNs lysate on BCYE plates.

To determine if glycolysis contributes to the ability of PMNs to rapidly kill *L. pneumophila*, PMNs were pretreated with 1 mM 2-deoxyglucose prior to infection. PMNs were plated into 24-well plates containing glass coverslips (3×10^6 cells per well) and infected with either post-exponential-phase wild type, $\Delta T4SS$, $\Delta lamA$, the complemented *lamA/C* or formalin-killed wild-type bacteria at an MOI of 1. Following 15 min infection, monolayers were fixed and processed for confocal microscopy as described above.

Mouse infection model. Female specific-pathogen-free, 6- to 8-week-old A/J mice were housed in specific-pathogen-free conditions within the animal care facility of the Faculty of Medicine, University of Rijeka, according to standard guidelines, and the use of animals for infection was approved by the Institutional Animal Care and Use Committee (IACUC). The incision was made through the skin of the ventral neck, the trachea was isolated, and 50 μ l of the bacterial suspension in sterile saline was inoculated using a 26-gauge needle followed by 10 to 20 μ l of air by intratracheal infection. A/J mice were inoculated with *L. pneumophila* (10^6 CFU per mouse) wild type or $\Delta lamA$ mutant. The skin incision was surgically closed. At 4 and 12 h postinoculation, the mice were euthanized, and the lung was removed. The lungs were excised, minced, and incubated in RPMI 1640 medium containing 5% fetal calf serum (FCS), 1 mg of collagenase A (Sigma Chemical Company, St. Louis, MO) per ml, and 20 μ l DNase per ml (Sigma Chemical Company, St. Louis, MO) for 60 min at 37°C in a shaking incubator. The cells were further disaggregated by drawing the lung homogenate repeatedly through the cell strainer prior to pelleting of the cells by centrifugation. Finally, the cells were resuspended in PBS containing 2% FCS and 1 mM EDTA. Isolation of neutrophils was performed by EasyStep mouse neutrophil enrichment kit (Stemcell Technologies, Canada), according to the manufacturer's instructions, by immunomagnetic-negative selection. The cells were phenotyped using monoclonal antibodies specific for the following cell surface antigens: anti-CD11b (BD, Bioscience, USA) and anti-Ly6g⁺ (eBioscience, USA). The immunofluorescence analysis was performed by BD fluorescence-activated cell sorter (FACS) Aria III flow cytometer using FACSDiva software. For determination of bacterial number within the neutrophils, the neutrophils were isolated as previously described, followed by treatment with Triton X-100. The suspension was plated on the BCYE agar and the number of bacteria determined by CFU.

Recruitment of p47phox, lactoferrin, and elastase to the *L. pneumophila* phagosome. To determine if the NADPH oxidase complex, specific, and azurophilic granules are recruited to the *L. pneumophila* phagosome, PMNs were plated into 24-well plates containing glass coverslips (3×10^6 cells per well) and infected with either post-exponential-phase wild type, the $\Delta T4SS$ and $\Delta lamA$ mutants, or the

complemented *lamA/C* mutant at an MOI of 1. Additionally, killed and opsonized *S. aureus* was used as a positive control for marker recruitment. At 5, 15, and 60 min postinfection, the monolayers were fixed with 4% formaldehyde for 30 min and permeabilized with 0.1% Triton X-100 in PBS for 15 min. The monolayers were labeled with rabbit anti-*Legionella* antiserum (1:1,000 dilution) in conjunction with mouse anti-p47phox (BD Transduction Laboratories), anti-lactoferrin (Abcam), or anti-elastase (Abcam) antibodies. PMNs were infected with bacteria and analyzed by confocal microscopy.

Intracellular respiratory burst response. A kinetic intracellular reactive oxygen species (ROS) production in neutrophils was measured as previously described (91) with modifications. Neutrophils (4×10^5) were plated in 96-well white plates, and intracellular ROS was detected by 125 μ M luminol in the presence of 75 μ g/ml of superoxide dismutase. Cells were stimulated with 300 nM phorbol myristate acetate (PMA) and infected with the wild type or different mutants of *L. pneumophila* at an MOI of 5:1 (106, 107). After the addition of phagocytic stimuli, plates were spun at room temperature at $600 \times g$ for 4 min at 14°C and immediately placed in a SpectraMax L luminometer (Molecular Devices, Sunnyvale, CA, USA). Total integrated relative light units (RLUs) at 37°C were determined for 90 min using SoftMax Pro software (Molecular Devices) (108, 109). The data are represented as area under the curve from three different experiments.

The nitroblue tetrazolium (NBT) assay was also used to visualize intracellular superoxide radical production induced by the wild-type strain or different mutants of *L. pneumophila*. Neutrophils (1×10^6 cells/ml) attached to plasma-coated glass coverslips were unstimulated or stimulated with the wild-type strain or the different mutants of *L. pneumophila* at an MOI of 5:1. Phagocytosis was synchronized at $600 \times g$ and 14°C for 4 min, and cells were incubated at 37°C in 5% CO₂ for 60 min in RPMI containing NBT. After incubation, cells were fixed with methanol followed by staining of *L. pneumophila* using antibodies. The confocal images showed reduced NBT precipitates as black deposits.

SUPPLEMENTAL MATERIAL

Supplemental material is available online only.

FIG S1, TIF file, 1 MB.

FIG S2, TIF file, 0.5 MB.

FIG S3, TIF file, 0.1 MB.

FIG S4, TIF file, 0.7 MB.

ACKNOWLEDGMENTS

Y.A.K. is supported by the National Institutes of Health awards R01AI 140195 and R21AI 142727, and by the Commonwealth of Kentucky Research Challenge Trust Fund. M.S. is funded by the Croatian Science Foundation grants HRZZ-IP-2016-9003 and UNIRI-biomed-128. S.U. is funded by National Institutes of Health award R21AI 142727. The funders had no role in study design, data collection and analysis, decision to publish, or preparation of the manuscript.

We declare that no competing interests exist.

C.T.D.P., A.V., H.E.H., and M.O. performed the experiments; C.T.D.P., A.V., H.E.H., M.O., M.S., S.U., and Y.A.K. analyzed the data; and Y.A.K. supervised the project. All authors wrote the manuscript.

REFERENCES

- Fields BS. 1996. The molecular ecology of legionellae. *Trends Microbiol* 4:286–290. [https://doi.org/10.1016/0966-842x\(96\)10041-x](https://doi.org/10.1016/0966-842x(96)10041-x).
- Molmeret M, Horn M, Wagner M, Santic M, Abu Kwaik Y. 2005. Amoebae as training grounds for intracellular bacterial pathogens. *Appl Environ Microbiol* 71:20–28. <https://doi.org/10.1128/AEM.71.1.20-28.2005>.
- Harb OS, Gao L-Y, Abu Kwaik Y. 2000. From protozoa to mammalian cells: a new paradigm in the life cycle of intracellular bacterial pathogens. *Environ Microbiol* 2:251–265. <https://doi.org/10.1046/j.1462-2920.2000.00112.x>.
- Desai SK, Kenney LJ. 2019. Switching lifestyles is an in vivo adaptive strategy of bacterial pathogens. *Front Cell Infect Microbiol* 9:421. <https://doi.org/10.3389/fcimb.2019.00421>.
- Shuman HA, Purcell M, Segal G, Hales L, Wiater LA. 1998. Intracellular multiplication of *Legionella pneumophila*: human pathogen or accidental tourist? *Curr Top Microbiol Immunol* 225:99–112. https://doi.org/10.1007/978-3-642-80451-9_6.
- Best A, Abu Kwaik Y. 2018. Evolution of the arsenal of *Legionella pneumophila* effectors to modulate protist hosts. *mBio* 9:e01313-18. <https://doi.org/10.1128/mBio.01313-18>.
- Rechnitzer C, Blom J. 1989. Engulfment of the Philadelphia strain of *Legionella pneumophila* within pseudopod coils in human phagocytes. Comparison with the other *Legionella* strains and species. *APMIS* 97:105–114. <https://doi.org/10.1111/j.1699-0463.1989.tb00763.x>.
- Horwitz MA. 1984. Phagocytosis of the Legionnaires' disease bacterium (*Legionella pneumophila*) occurs by a novel mechanism: engulfment within a pseudopod coil. *Cell* 36:27–33. [https://doi.org/10.1016/0092-8674\(84\)90070-9](https://doi.org/10.1016/0092-8674(84)90070-9).
- Horwitz MA, Silverstein SC. 1980. Legionnaires' disease bacterium (*Legionella pneumophila*) multiples intracellularly in human monocytes. *J Clin Invest* 66:441–450. <https://doi.org/10.1172/JCI109874>.
- Horwitz MA. 1983. The Legionnaires' disease bacterium (*Legionella pneumophila*) inhibits phagosome-lysosome fusion in human monocytes. *J Exp Med* 158:2108–2126. <https://doi.org/10.1084/jem.158.6.2108>.
- Horwitz MA. 1983. Formation of a novel phagosome by the Legionnaires' disease bacterium (*Legionella pneumophila*) in human monocytes. *J Exp Med* 158:1319–1331. <https://doi.org/10.1084/jem.158.4.1319>.
- Ziltener P, Reinheckel T, Oxenius A. 2016. Neutrophil and alveolar macrophage-mediated innate immune control of *Legionella pneumophila* lung

- infection via TNF and ROS. *PLoS Pathog* 12:e1005591. <https://doi.org/10.1371/journal.ppat.1005591>.
13. Horwitz MA, Silverstein SC. 1981. Interaction of the Legionnaires' disease bacterium (*Legionella pneumophila*) with human phagocytes. I. *L. pneumophila* resists killing by polymorphonuclear leukocytes, antibody, and complement. *J Exp Med* 153:386–397. <https://doi.org/10.1084/jem.153.2.386>.
 14. Brown AS, Yang C, Hartland EL, van Driel IR. 2017. The regulation of acute immune responses to the bacterial lung pathogen *Legionella pneumophila*. *J Leukoc Biol* 101:875–886. <https://doi.org/10.1189/jlb.4MR0816-340R>.
 15. Brown AS, Yang C, Fung KY, Bachem A, Bourges D, Bedoui S, Hartland EL, van Driel IR. 2016. Cooperation between monocyte-derived cells and lymphoid cells in the acute response to a bacterial lung pathogen. *PLoS Pathog* 12:e1005691. <https://doi.org/10.1371/journal.ppat.1005691>.
 16. Copenhaver AM, Casson CN, Nguyen HT, Duda MM, Shin S. 2015. IL-1R signaling enables bystander cells to overcome bacterial blockade of host protein synthesis. *Proc Natl Acad Sci U S A* 112:7557–7562. <https://doi.org/10.1073/pnas.1501289112>.
 17. Copenhaver AM, Casson CN, Nguyen HT, Fung TC, Duda MM, Roy CR, Shin S. 2014. Alveolar macrophages and neutrophils are the primary reservoirs for *Legionella pneumophila* and mediate cytosolic surveillance of type IV secretion. *Infect Immun* 82:4325–4336. <https://doi.org/10.1128/IAI.01891-14>.
 18. Casson CN, Doerner JL, Copenhaver AM, Ramirez J, Holmgren AM, Boyer MA, Siddarthan IJ, Rouhanifard SH, Raj A, Shin S. 2017. Neutrophils and Ly6Chi monocytes collaborate in generating an optimal cytokine response that protects against pulmonary *Legionella pneumophila* infection. *PLoS Pathog* 13:e1006309. <https://doi.org/10.1371/journal.ppat.1006309>.
 19. Cai S, Batra S, Langohr I, Iwakura Y, Jeyaseelan S. 2016. IFN-gamma induction by neutrophil-derived IL-17A homodimer augments pulmonary antibacterial defense. *Mucosal Immunol* 9:718–729. <https://doi.org/10.1038/mi.2015.95>.
 20. Kubelkova K, Macela A. 2019. Innate immune recognition: an issue more complex than expected. *Front Cell Infect Microbiol* 9:241. <https://doi.org/10.3389/fcimb.2019.00241>.
 21. Leseigneur C, Le-Bury P, Pizarro-Cerda J, Dussurget O. 2020. Emerging evasion mechanisms of macrophage defenses by pathogenic bacteria. *Front Cell Infect Microbiol* 10:577559. <https://doi.org/10.3389/fcimb.2020.577559>.
 22. Mnich ME, van Dalen R, van Sorge NM. 2020. C-type lectin receptors in host defense against bacterial pathogens. *Front Cell Infect Microbiol* 10:309. <https://doi.org/10.3389/fcimb.2020.00309>.
 23. Szulc-Dąbrowska L, Bossowska-Nowicka M, Struzik J, Toka FN. 2020. Cathepsins in bacteria-macrophage interaction: defenders or victims of circumstance? *Front Cell Infect Microbiol* 10:601072. <https://doi.org/10.3389/fcimb.2020.601072>.
 24. Sachdeva K, Sundaramurthy V. 2020. The interplay of host lysosomes and intracellular pathogens. *Front Cell Infect Microbiol* 10:595502. <https://doi.org/10.3389/fcimb.2020.595502>.
 25. Snaka T, Fasel N. 2020. Behind the scenes: nod-like receptor X1 controls inflammation and metabolism. *Front Cell Infect Microbiol* 10:609812. <https://doi.org/10.3389/fcimb.2020.609812>.
 26. Samir P, Malireddi RKS, Kanneganti TD. 2020. The PANoptosome: a deadly protein complex driving pyroptosis, apoptosis, and necroptosis (PANoptosis). *Front Cell Infect Microbiol* 10:238. <https://doi.org/10.3389/fcimb.2020.00238>.
 27. Christgen S, Zheng M, Kesavardhana S, Karki R, Malireddi RKS, Banoth B, Place DE, Briard B, Sharma BR, Tuladhar S, Samir P, Burton A, Kanneganti TD. 2020. Identification of the PANoptosome: a molecular platform triggering pyroptosis, apoptosis, and necroptosis (PANoptosis). *Front Cell Infect Microbiol* 10:237. <https://doi.org/10.3389/fcimb.2020.00237>.
 28. Malireddi RKS, Kesavardhana S, Kanneganti TD. 2019. ZBP1 and TAK1: master regulators of NLRP3 inflammasome/pyroptosis, apoptosis, and necroptosis (PAN-optosis). *Front Cell Infect Microbiol* 9:406. <https://doi.org/10.3389/fcimb.2019.00406>.
 29. Baskerville A, Fitzgeorge RB, Broster M, Hambleton P. 1983. Histopathology of experimental Legionnaires' disease in guinea pigs, rhesus monkeys and marmosets. *J Pathol* 139:349–362. <https://doi.org/10.1002/path.1711390310>.
 30. Blackmon JA, Hicklin MD, Chandler FW. 1978. Legionnaires' disease. Pathological and historical aspects of a 'new' disease. *Arch Pathol Lab Med* 102:337–343.
 31. Carrington CB. 1979. Pathology of Legionnaires' disease. *Ann Intern Med* 90:496–499. <https://doi.org/10.7326/0003-4819-90-4-496>.
 32. Chandler FW, McDade JE, Hicklin MD, Blackmon JA, Thomason BM, Ewing EP, Jr. 1979. Pathologic findings in guinea pigs inoculated intraperitoneally with the Legionnaires' disease bacterium. *Ann Intern Med* 90:671–675. <https://doi.org/10.7326/0003-4819-90-4-671>.
 33. Edelstein PH. 1993. Legionnaires' disease. *Clin Infect Dis* 16:741–747. <https://doi.org/10.1093/clind/16.6.741>.
 34. Edelstein PH, Meyer RD. 1984. Legionnaires' disease. A review. *Chest* 85:114–120. <https://doi.org/10.1378/chest.85.1.114>.
 35. Fields BS, Benson RF, Besser RE. 2002. *Legionella* and Legionnaires' disease: 25 years of investigation. *Clin Microbiol Rev* 15:506–526. <https://doi.org/10.1128/cmr.15.3.506-526.2002>.
 36. Qiu J, Luo ZQ. 2017. *Legionella* and *Coxiella* effectors: strength in diversity and activity. *Nat Rev Microbiol* 15:591–605. <https://doi.org/10.1038/nrmicro.2017.67>.
 37. Isberg RR, O'Connor TJ, Heidtman M. 2009. The *Legionella pneumophila* replication vacuole: making a cosy niche inside host cells. *Nat Rev Microbiol* 7:13–24. <https://doi.org/10.1038/nrmicro1967>.
 38. Kitao T, Nagai H, Kubori T. 2020. Divergence of *Legionella* effectors reversing conventional and unconventional ubiquitination. *Front Cell Infect Microbiol* 10:448. <https://doi.org/10.3389/fcimb.2020.00448>.
 39. Li P, Vassiliadis D, Ong SY, Bennett-Wood V, Sugimoto C, Yamagishi J, Hartland EL, Pasricha S. 2020. *Legionella pneumophila* infection rewires the *Acanthamoeba castellanii* Transcriptome, highlighting a class of sir-tuin genes. *Front Cell Infect Microbiol* 10:428. <https://doi.org/10.3389/fcimb.2020.00428>.
 40. Younes S, Al-Sulaiti A, Nasser EAA, Najjar H, Kamareddine L. 2020. *Drosophila* as a model organism in host-pathogen interaction studies. *Front Cell Infect Microbiol* 10:214. <https://doi.org/10.3389/fcimb.2020.00214>.
 41. Thomas DR, Newton P, Lau N, Newton HJ. 2020. Interfering with autophagy: the opposing strategies deployed by *Legionella pneumophila* and *Coxiella burnetii* effector proteins. *Front Cell Infect Microbiol* 10:599762. <https://doi.org/10.3389/fcimb.2020.599762>.
 42. LeibundGut-Landmann S, Weidner K, Hilbi H, Oxenius A. 2011. Nonhematopoietic cells are key players in innate control of bacterial airway infection. *J Immunol* 186:3130–3137. <https://doi.org/10.4049/jimmunol.1003565>.
 43. Miralda I, Uriarte SM, McLeish KR. 2017. Multiple phenotypic changes define neutrophil priming. *Front Cell Infect Microbiol* 7:217. <https://doi.org/10.3389/fcimb.2017.00217>.
 44. Nguyen GT, Green ER, Meccas J. 2017. Neutrophils to the ROScUE: mechanisms of NADPH oxidase activation and bacterial resistance. *Front Cell Infect Microbiol* 7:373. <https://doi.org/10.3389/fcimb.2017.00373>.
 45. Puerta-Arias JD, Mejia SP, Gonzalez A. 2020. The role of the interleukin-17 axis and neutrophils in the pathogenesis of endemic and systemic mycoses. *Front Cell Infect Microbiol* 10:595301. <https://doi.org/10.3389/fcimb.2020.595301>.
 46. Wei Z, Wang Z, Liu X, Wang C, Han Z, Wu D, Zhang Y, Zhang X, Yang Z, Liu Q. 2020. *Toxoplasma gondii* triggers neutrophil extracellular traps release in dogs. *Front Cell Infect Microbiol* 10:429. <https://doi.org/10.3389/fcimb.2020.00429>.
 47. Peng L, Li L, He XL, Yu JY, Zeng ZJ, Yang WJ, Zhang B, Zhang TS, Cao H, Huang SH, Liu LQ. 2020. Memantine displays antimicrobial activity by enhancing *Escherichia coli* pathogen-induced formation of neutrophil extracellular traps. *Front Cell Infect Microbiol* 10:47. <https://doi.org/10.3389/fcimb.2020.00047>.
 48. Jacobs RF, Locksley RM, Wilson CB, Haas JE, Klebanoff SJ. 1984. Interaction of primate alveolar macrophages and *Legionella pneumophila*. *J Clin Invest* 73:1515–1523. <https://doi.org/10.1172/JCI11357>.
 49. Summersgill JT, Raff MJ, Miller RD. 1988. Interactions of virulent and avirulent *Legionella pneumophila* with human polymorphonuclear leukocytes. *Microb Pathog* 5:41–47. [https://doi.org/10.1016/0882-4010\(88\)90079-4](https://doi.org/10.1016/0882-4010(88)90079-4).
 50. Rehnitz C, Kharazmi A. 1992. Effect of *Legionella pneumophila* cytotoxic protease on human neutrophil and monocyte function. *Microb Pathog* 12:115–125. [https://doi.org/10.1016/0882-4010\(92\)90114-4](https://doi.org/10.1016/0882-4010(92)90114-4).
 51. Yamamoto Y, Klein TW, Brown K, Friedman H. 1992. Differential morphologic and metabolic alterations in permissive versus nonpermissive murine macrophages infected with *Legionella pneumophila*. *Infect Immun* 60:3231–3237. <https://doi.org/10.1128/IAI.60.8.3231-3237.1992>.
 52. Jacob T, Escallier JC, Sanguedolce MV, Chicheportiche C, Bongrand P, Capo C, Mege JL. 1994. *Legionella pneumophila* inhibits superoxide generation in human monocytes via the down-modulation of a and b

- protein kinase C isoforms. *J Leukoc Biol* 55:310–312. <https://doi.org/10.1002/jlb.55.3.310>.
53. Sahney NN, Summersgill JT, Ramirez JA, Miller RD. 2001. Inhibition of oxidative burst and chemotaxis in human phagocytes by *Legionella pneumophila* zinc metalloprotease. *J Med Microbiol* 50:517–525. <https://doi.org/10.1099/0022-1317-50-6-517>.
 54. Rechnitzer C, Kharazmi A, Nielsen H, Baek L. 1987. Modulation of human neutrophil and monocyte oxidative burst by *Legionella pneumophila* sonic extract. *Eur J Clin Microbiol* 6:646–652. <https://doi.org/10.1007/BF02013061>.
 55. Horwitz MA, Silverstein SC. 1981. Interaction of the legionnaires' disease bacterium (*Legionella pneumophila*) with human phagocytes. II. Antibody promotes binding of *L. pneumophila* to monocytes but does not inhibit intracellular multiplication. *J Exp Med* 153:398–406. <https://doi.org/10.1084/jem.153.2.398>.
 56. Curto P, Riley SP, Simoes I, Martinez JJ. 2019. Macrophages infected by a pathogen and a non-pathogen spotted fever group *Rickettsia* reveal differential reprogramming signatures early in infection. *Front Cell Infect Microbiol* 9:97. <https://doi.org/10.3389/fcimb.2019.00097>.
 57. Çakır T, Panagiotou G, Uddin R, Durmuş S. 2020. Novel approaches for systems biology of metabolism-oriented pathogen-human interactions: a mini-review. *Front Cell Infect Microbiol* 10:52. <https://doi.org/10.3389/fcimb.2020.00052>.
 58. Sharma PV, Thaiss CA. 2020. Host-microbiome interactions in the era of single-cell biology. *Front Cell Infect Microbiol* 10:569070. <https://doi.org/10.3389/fcimb.2020.569070>.
 59. Cumming BM, Pacl HT, Steyn AJC. 2020. Relevance of the Warburg effect in tuberculosis for host-directed therapy. *Front Cell Infect Microbiol* 10:576596. <https://doi.org/10.3389/fcimb.2020.576596>.
 60. Eisenreich W, Rudel T, Heesemann J, Goebel W. 2019. How viral and intracellular bacterial pathogens reprogram the metabolism of host cells to allow their intracellular replication. *Front Cell Infect Microbiol* 9:42. <https://doi.org/10.3389/fcimb.2019.00042>.
 61. Yu Q, Wang Y, Dong L, He Y, Liu R, Yang Q, Cao Y, Wang Y, Jia A, Bi Y, Liu G. 2020. Regulations of glycolytic activities on macrophages functions in tumor and infectious inflammation. *Front Cell Infect Microbiol* 10:287. <https://doi.org/10.3389/fcimb.2020.00287>.
 62. Joshi MB, Lad A, Bharath Prasad AS, Balakrishnan A, Ramachandra L, Satyamoorthy K. 2013. High glucose modulates IL-6 mediated immune homeostasis through impeding neutrophil extracellular trap formation. *FEBS Lett* 587:2241–2246. <https://doi.org/10.1016/j.febslet.2013.05.053>.
 63. De Toni S, Piva E, Lapolla A, Fontana G, Fedele D, Plebani M. 1997. Respiratory burst of neutrophils in diabetic patients with periodontal disease. *Ann N Y Acad Sci* 832:363–367. <https://doi.org/10.1111/j.1749-6632.1997.tb46264.x>.
 64. Hand WL, Hand DL, Vasquez Y. 2007. Increased polymorphonuclear leukocyte respiratory burst function in type 2 diabetes. *Diabetes Res Clin Pract* 76:44–50. <https://doi.org/10.1016/j.diabres.2006.07.015>.
 65. Rahman MA, Glasgow JN, Nadeem S, Reddy VP, Sevalkar RR, Lancaster JR, Jr., Steyn AJC. 2020. The role of host-generated H2S in microbial pathogenesis: new perspectives on tuberculosis. *Front Cell Infect Microbiol* 10:586923. <https://doi.org/10.3389/fcimb.2020.586923>.
 66. Zhu L, Zhao Q, Yang T, Ding W, Zhao Y. 2015. Cellular metabolism and macrophage functional polarization. *Int Rev Immunol* 34:82–100. <https://doi.org/10.3109/08830185.2014.969421>.
 67. Jha AK, Huang SC, Sergushichev A, Lampropoulou V, Ivanova Y, Loginicheva E, Chmielewski K, Stewart KM, Ashall J, Everts B, Pearce EJ, Driggers EM, Artyomov MN. 2015. Network integration of parallel metabolic and transcriptional data reveals metabolic modules that regulate macrophage polarization. *Immunity* 42:419–430. <https://doi.org/10.1016/j.immuni.2015.02.005>.
 68. O'Neill LA, Pearce EJ. 2016. Immunometabolism governs dendritic cell and macrophage function. *J Exp Med* 213:15–23. <https://doi.org/10.1084/jem.20151570>.
 69. Murray PJ, Rathmell J, Pearce E. 2015. SnapShot: immunometabolism. *Cell Metab* 22:190–190.e1. <https://doi.org/10.1016/j.cmet.2015.06.014>.
 70. Eisenreich W, Rudel T, Heesemann J, Goebel W. 2017. To eat and to be eaten: mutual metabolic adaptations of immune cells and intracellular bacterial pathogens upon infection. *Front Cell Infect Microbiol* 7. <https://doi.org/10.3389/fcimb.2017.00316>.
 71. Bradshaw EM, Raddassi K, Elyaman W, Orban T, Gottlieb PA, Kent SC, Hafler DA. 2009. Monocytes from patients with type 1 diabetes spontaneously secrete proinflammatory cytokines inducing Th17 cells. *J Immunol* 183:4432–4439. <https://doi.org/10.4049/jimmunol.0900576>.
 72. Torres-Castro I, Arroyo-Camarena ÚD, Martínez-Reyes CP, Gómez-Arauz AY, Dueñas-Andrade Y, Hernández-Ruiz J, Béjar YL, Zaga-Clavellina V, Morales-Montor J, Terrazas LI, Kzhyshkowska J, Escobedo G. 2016. Human monocytes and macrophages undergo M1-type inflammatory polarization in response to high levels of glucose. *Immunology Lett* 176:81–89. <https://doi.org/10.1016/j.imlet.2016.06.001>.
 73. Kraakman MJ, Murphy AJ, Jandeleit-Dahm K, Kammoun HL. 2014. Macrophage polarization in obesity and type 2 diabetes: weighing down our understanding of macrophage function? *Front Immunol* 5:470. <https://doi.org/10.3389/fimmu.2014.00470>.
 74. Haidet J, Cifarelli V, Trucco M, Luppi P. 2012. C-peptide reduces pro-inflammatory cytokine secretion in LPS-stimulated U937 monocytes in condition of hyperglycemia. *Inflamm Res* 61:27–35. <https://doi.org/10.1007/s00011-011-0384-8>.
 75. Pan Y, Wang Y, Cai L, Cai Y, Hu J, Yu C, Li J, Feng Z, Yang S, Li X, Liang G. 2012. Inhibition of high glucose-induced inflammatory response and macrophage infiltration by a novel curcumin derivative prevents renal injury in diabetic rats. *British J Pharmacol* 166:1169–1182. <https://doi.org/10.1111/j.1476-5381.2012.01854.x>.
 76. Reinhold D, Ansoorge S, Schleicher ED. 1996. Elevated glucose levels stimulate transforming growth factor-beta 1 (TGF-beta 1), suppress interleukin IL-2, IL-6 and IL-10 production and DNA synthesis in peripheral blood mononuclear cells. *Horm Metab Res* 28:267–270. <https://doi.org/10.1055/s-2007-979789>.
 77. Erbel C, Rupp G, Domschke G, Linden F, Akhavanpoor M, Doesch AO, Katus HA, Gleissner CA. 2016. Differential regulation of aldose reductase expression during macrophage polarization depends on hyperglycemia. *Innate Immun* 22:230–237. <https://doi.org/10.1177/1753425916632053>.
 78. Freereman AJ, Johnson AR, Sacks GN, Milner JJ, Kirk EL, Troester MA, Macintyre AN, Goraksha-Hicks P, Rathmell JC, Makowski L. 2014. Metabolic reprogramming of macrophages: glucose transporter 1 (GLUT1)-mediated glucose metabolism drives a proinflammatory phenotype. *J Biol Chem* 289:7884–7896. <https://doi.org/10.1074/jbc.M113.522037>.
 79. Ham M, Lee JW, Choi AH, Jang H, Choi G, Park J, Kozuka C, Sears DD, Masuzaki H, Kim JB. 2013. Macrophage glucose-6-phosphate dehydrogenase stimulates proinflammatory responses with oxidative stress. *Mol Cell Biol* 33:2425–2435. <https://doi.org/10.1128/MCB.01260-12>.
 80. Baillet A, Hograindleur MA, El Benna J, Grichine A, Berthier S, Morel F, Pacllet MH. 2017. Unexpected function of the phagocyte NADPH oxidase in supporting hyperglycolysis in stimulated neutrophils: key role of 6-phosphofructo-2-kinase. *FASEB J* 31:663–673. <https://doi.org/10.1096/fj.201600720R>.
 81. Tsai TF, Finn DR, Plikaytis BD, McCauley W, Martin SM, Fraser DW. 1979. Legionnaires' disease: clinical features of the epidemic in Philadelphia. *Ann Intern Med* 90:509–517. <https://doi.org/10.7326/0003-4819-90-4-509>.
 82. Hicklin MD, Thomason BM, Chandler FW, Blackmon JA. 1980. Pathogenesis of acute Legionnaires' disease pneumonia. *Am J Clin Pathol* 73:480–487. <https://doi.org/10.1093/ajcp/73.4.480>.
 83. Cunha BA, Burillo A, Bouza E. 2016. Legionnaires' disease. *Lancet* 387:376–385. [https://doi.org/10.1016/S0140-6736\(15\)60078-2](https://doi.org/10.1016/S0140-6736(15)60078-2).
 84. Iyer NV, Kotch LE, Agani F, Leung SW, Laughner E, Wenger RH, Gassmann M, Gearhart JD, Lawler AM, Yu AY, Semenza GL. 1998. Cellular and developmental control of O2 homeostasis by hypoxia-inducible factor 1 alpha. *Genes Dev* 12:149–162. <https://doi.org/10.1101/gad.12.2.149>.
 85. Brandt SL, Serezani CH. 2017. Too much of a good thing: how modulating LTB4 actions restore host defense in homeostasis or disease. *Semin Immunol* 33:37–43. <https://doi.org/10.1016/j.smim.2017.08.006>.
 86. Dhainaut J-F, Claessens Y-E, Janes J, Nelson DR. 2005. Underlying disorders and their impact on the host response to infection. *Clin Infect Dis* 41:S481–S489. <https://doi.org/10.1086/432001>.
 87. Prats C, Graham TE, Shearer J. 2018. The dynamic life of the glycogen granule. *J Biol Chem* 293:7089–7098. <https://doi.org/10.1074/jbc.R117.802843>.
 88. Price C, Jones S, Mihelcic M, Santic M, Abu Kwaik Y. 2020. Paradoxical pro-inflammatory responses by human macrophages to an amoebae host-adapted *Legionella* effector. *Cell Host Microbe* 27:571–584.e7. <https://doi.org/10.1016/j.chom.2020.03.003>.
 89. Verbrugh HA, Lee DA, Elliott GR, Keane WF, Hoidal JR, Peterson PK. 1985. Opsonization of *Legionella pneumophila* in human serum: key roles for specific antibodies and the classical complement pathway. *Immunology* 54:643–653.
 90. Price JV, Jiang K, Galantowicz A, Freifeld A, Vance RE. 2018. *Legionella pneumophila* is directly sensitive to 2-deoxyglucose-phosphate via its

- UhpC transporter but is indifferent to shifts in host cell glycolytic metabolism. *J Bacteriol* 200:e00176-18. <https://doi.org/10.1128/JB.00176-18>.
91. Bagaitkar J, Barbu EA, Perez-Zapata LJ, Austin A, Huang G, Pallat S, Dinuer MC. 2017. PI(3)P-p40phox binding regulates NADPH oxidase activation in mouse macrophages and magnitude of inflammatory responses in vivo. *J Leukoc Biol* 101:449–457. <https://doi.org/10.1189/jlb.3AB0316-139R>.
 92. Cornejo E, Schlaermann P, Mukherjee S. 2017. How to rewire the host cell: a home improvement guide for intracellular bacteria. *J Cell Biol* 216:3931–3948. <https://doi.org/10.1083/jcb.201701095>.
 93. Price JV, Vance RE. 2014. The macrophage paradox. *Immunity* 41:685–693. <https://doi.org/10.1016/j.immuni.2014.10.015>.
 94. O'Connor TJ, Adepoju Y, Boyd D, Isberg RR. 2011. Minimization of the *Legionella pneumophila* genome reveals chromosomal regions involved in host range expansion. *Proc Natl Acad Sci U S A* 108:14733–14740. <https://doi.org/10.1073/pnas.1111678108>.
 95. Hodgson K, Morris J, Bridson T, Govan B, Rush C, Ketheesan N. 2015. Immunological mechanisms contributing to the double burden of diabetes and intracellular bacterial infections. *Immunology* 144:171–85. <https://doi.org/10.1111/imm.12394>.
 96. Neumeister B, Faigle M, Sommer M, Zähringer U, Stelter F, Menzel R, Schütt C, Northoff H. 1998. Low endotoxic potential of *Legionella pneumophila* lipopolysaccharide due to failure of interaction with the monocyte lipopolysaccharide receptor CD14. *Infect Immun* 66:4151–4157. <https://doi.org/10.1128/IAI.66.9.4151-4157.1998>.
 97. Sory MP, Cornelis GR. 1994. Translocation of a hybrid YopE-adenylate cyclase from *Yersinia enterocolitica* into HeLa cells. *Mol Microbiol* 14:583–594. <https://doi.org/10.1111/j.1365-2958.1994.tb02191.x>.
 98. Price CT, Al-Khodori S, Al-Quadan T, Santic M, Habyarimana F, Kalia A, Kwaik YA. 2009. Molecular mimicry by an F-box effector of *Legionella pneumophila* hijacks a conserved polyubiquitination machinery within macrophages and protozoa. *PLoS Pathog* 5:e1000704. <https://doi.org/10.1371/journal.ppat.1000704>.
 99. Sun L, Yang S, Deng Q, Dong K, Li Y, Wu S, Huang R. 2020. *Salmonella* effector SpvB disrupts intestinal epithelial barrier integrity for bacterial translocation. *Front Cell Infect Microbiol* 10:606541. <https://doi.org/10.3389/fcimb.2020.606541>.
 100. Nakamura-Tsuruta S, Yasuda M, Nakamura T, Shinoda E, Furuyashiki T, Kakutani R, Takata H, Kato Y, Ashida H. 2012. Comparative analysis of carbohydrate-binding specificities of two anti-glycogen monoclonal antibodies using ELISA and surface plasmon resonance. *Carbohydr Res* 350:49–54. <https://doi.org/10.1016/j.carres.2011.12.029>.
 101. Balci A, Solano-Collado V, Baldassarre M, Spano S. 2020. VARP and Rab9 are dispensable for the Rab32/BLOC-3 dependent *Salmonella* killing. *Front Cell Infect Microbiol* 10:581024. <https://doi.org/10.3389/fcimb.2020.581024>.
 102. Masud S, van der Burg L, Storm L, Prajsnar TK, Meijer AH. 2019. Rubicon-dependent Lc3 recruitment to *Salmonella*-containing phagosomes is a host defense mechanism triggered independently from major bacterial virulence factors. *Front Cell Infect Microbiol* 9:279. <https://doi.org/10.3389/fcimb.2019.00279>.
 103. Guo Q, Bi J, Li M, Ge W, Xu Y, Fan W, Wang H, Zhang X. 2019. ESX secretion-associated protein C from *Mycobacterium tuberculosis* induces macrophage activation through the Toll-like receptor-4/mitogen-activated protein kinase signaling pathway. *Front Cell Infect Microbiol* 9:158. <https://doi.org/10.3389/fcimb.2019.00158>.
 104. Mambu J, Barilleau E, Fragnet-Trapp L, Le Vern Y, Olivier M, Sadrin G, Grepinet O, Taieb F, Velge P, Wiedemann A. 2020. Rck of *Salmonella* Typhimurium delays the host cell cycle to facilitate bacterial invasion. *Front Cell Infect Microbiol* 10:586934. <https://doi.org/10.3389/fcimb.2020.586934>.
 105. Gan J, Scott NE, Newson JPM, Wibawa RR, Wong Fok Lung T, Pollock GL, Ng GZ, van Driel I, Pearson JS, Hartland EL, Giogha C. 2020. The *Salmonella* effector SseK3 targets small Rab GTPases. *Front Cell Infect Microbiol* 10:419. <https://doi.org/10.3389/fcimb.2020.00419>.
 106. Garg R, Borbora SM, Bansia H, Rao S, Singh P, Verma R, Balaji KN, Nagaraja V. 2020. *Mycobacterium tuberculosis* calcium pump CtpF modulates the autophagosome in an mTOR-dependent manner. *Front Cell Infect Microbiol* 10:461. <https://doi.org/10.3389/fcimb.2020.00461>.
 107. Green RS, Izac JR, Naimi WA, O'Bier N, Breitschwerdt EB, Marconi RT, Carlyon JA. 2020. *Ehrlichia chaffeensis* EplA interaction with host cell protein disulfide isomerase promotes infection. *Front Cell Infect Microbiol* 10:500. <https://doi.org/10.3389/fcimb.2020.00500>.
 108. Kunz TC, Gotz R, Sauer M, Rudel T. 2019. Detection of *Chlamydia* developmental forms and secreted effectors by expansion microscopy. *Front Cell Infect Microbiol* 9:276. <https://doi.org/10.3389/fcimb.2019.00276>.
 109. Wang X, Sun J, Wan L, Yang X, Lin H, Zhang Y, He X, Zhong H, Guan K, Min M, Sun Z, Yang X, Wang B, Dong M, Wei C. 2020. The *Shigella* type III secretion effector IpaH4.5 targets NLRP3 to activate inflammasome signaling. *Front Cell Infect Microbiol* 10:511798. <https://doi.org/10.3389/fcimb.2020.511798>.